To - TIC

MASSACHUSETTS INSTITUTE OF TECHNOLOGY

CAMBRIDGE, MASSACHUSETTS 02139

Laboratory for
Manufacturing and
Productivity

School of Engineering

DOE/ER/10474--4

DE83 017012

FINAL REPORT
#DOE-ER-10474 - 4
for

IMPROVEMENT OF RELIABILITY OF WELDING BY IN-PROCESS SENSING AND CONTROL (DEVELOPMENT OF SMART WELDING MACHINES FOR GIRTH WELDING OF PIPES)

D.O.E. Contract No. DE-AC02-79ER10474.A000
(M.I.T. OSP #88547)

April 1983

David E. Hardt
Koichi Masubuchi
Henry M. Paynter
William C. Unkel

OK 6-30-83
J. Weinberger
OPC-CH

DISCLAIMER

NOTICE

Foreword

This report describes the work done to develop closed-loop in-process control of the welding process as one technique to improve the reliability of welding. The work was funded by the U.S. D.O.E. under contract No. DE-AC02-79ER10474.A000. Dr. Oscar Manley of D.O.E. served as program monitor. The principal investigators of the work were Professors K. Masubuchi and H.M. Paynter. Professors W. Unkel and D.E. Hardt were associate investigators. The material contained in the report represents the work of the investigators above and also of the following staff, graduate and undergraduate students: Dr. V.J. Papazoglou; Dr. J. Converti, Ms. M. Zackenshouse, Mr. Y. Dror, Mr. M. Connaughton, Mr. J.J. Crothers, Mr. P.G. Edelstein, Mr. J. Weinert, Mr. D.A. Garlow and Mr. J.D. Reiff.

TABLE OF CONTENTS

ABSTRACT

Closed-loop control of the welding variables represents a promising, cost-effective approach to improving weld quality and therefore reducing the total cost of producing welded structures. The ultimate goal is to place all significant weld variables under direct closed-loop control; this contrasts with preprogrammed machines which place the welding equipment under control. As the first step, an overall strategy has been formulated and an investigation of weld pool geometry control for gas tungsten arc process has been completed. The research activities were divided roughly into the areas of arc phenomena, weld pool phenomena, sensing techniques and control activities.

The control strategy developed is to decouple and separately regulate key determinants of a "good" weld. Once the selection of the key determinants of a good weld has been made, closed-loop control requires four components: a) an on-line technique for sensing each control variable; b) a physically based but computationally simple model relating the weld variables to the process inputs; c) at least one control variable on the welding device for each weld variable being controlled; and d) a control algorithm that combines the above components to provide independent output variable control. These activities must develop in parallel; trial closed-loop control systems should be developed early to identify the required accuracy of the models and sensors and to identify control problems.

To establish fundamental knowledge necessary for this approach, the steady and transient thermal and fluid behavior of the arc was investigated to a) determine the effect of current pulsing on the weld pool shape and b) evaluate whether current pulsing can be used to obtain separate control of weld pool top width and penetration (or back bead width for a full penetration). The origin and magnitude of the plasma jet forces has been clearly and accurately shown and the momentum of the plasma jet measured using a novel magnetic deflection technique. The "stiffness" of an arc to deflection by external flows or magnetic field has been explained in terms of the momentum of the plasma jet. Experiments have shown that the response of the arc to step changes in current is strongly influenced by transient fluid phenomena. The transient studies were conducted with a transistor-based current regulator which was designed by Alexander Kusko, Inc. to our specifications. The device was capable of changing the current with a band width of >20 kHz.

Closed-loop control requires computationally simple models of the welding process since their computations must be performed in real-time. It is particularly important to predict how the weld pool shape varies with the welding equipment variables. A simple model was developed to predict the width and depth of a stationary weld puddle and the results compared with experimental data. The model included conduction heat transfer and convection heat transfer in the weld pool and conduction and radiation heat transfer from the solid plate. Results were not extensive, but indicated that the model might serve as a parameter indentification model in a closed-loop controller. Considerable additional work will be required, in particular the application to the moving weld pool configuration.

The weld geometry control activities have concentrated on the case of full penetration welds, and have included: a) development of a novel technique to detect weld pool mass without access to the rear of the weld, b) demonstration of a simple penetration control system based on arc-voltage sensing and c) implementation of a real-time control of back bead width. In the fully penetrated mode the weld pool is supported against gravity and plasma jet forces by surface tension forces. Experimental measurements have clearly established that the fully penetrated weld pool responds like a second-order mechanical system, as would be expected from a simple model of the mechanical response. The experimental measurements were made by varying the plasma jet momentum and detecting the corresponding motion of the weld pool. Spectral analysis of the pool motion clearly identified the natural frequency and the high frequency rolloff which characterize second order systems. Since the weld pool mass is directly related to the natural frequency and the surface tension, the technique gives an estimate of pool mass from simple topside measurements. Additional work is required to establish the use of the technique for moving weld pools and to develop real-time pool position sensing techniques. Nonetheless the technique shows promise as a sensor for weld pool size.

Two closed-loop control schemes were investigated experimentally, both attempting to control full penetration weld geometry. The first used the arc-length change at full penetration as feedback while the second directly measured (from the back side) the width of the back bead. Not surprisingly the former was very simple, but gave an oscillatory back bead that varied from partial to full penetration. However, the latter method has been quite successful in regulating bead width. Although it involves an impractical sensing method, the dynamics and control studies that have been performed have laid the groundwork for proper control system design once sensing methods have been perfected.

1. Introduction

Over the years, the cost of constructing critical welded structures has increased dramatically. A significant portion of the increase comes from required inspection and repair, while the direct cost of welding has increased only slightly. The quality of the original weld, however, determines the number and seriousness of defects and therefore partly determines the repair costs. Closed-loop control of the welding variables represents a promising cost-effective approach to improving weld quality and therefore reducing the total cost of producing welded structures. Such an automated welding system can also play a significant role in repair operations or other hazardous situations and can help alleviate the problem of unavailability of highly skilled welders.

In an effort to minimize some of the problems associated with welding, various types of semiautomatic welding machines have been developed over the past thirty years. While the label "automatic" has been attached to many welding systems, in many cases these are as primitive as a mechanized welding device or at best are a pre-programmed machine. In such machines the torch travel speed, the wire feed rate and the power source characteristics are pre-adjusted to values which, based upon experience for the particular situation, produce an acceptable weld. Feedback and self-regulation of the weld in the presence of a variety of external disturbances are absent in these systems.

While the need for automatic seam tracking and control of welding subsystems has been recognized for some time, the importance of automation centered around direct control of the critical weld variables has only recently been recognized. A strong indication of this interest was shown by the public session of the 1979 Annual Meeting of the International Institute of Welding devoted to "Welding Processes and Workshop Automation" [1.1]. Some feedback control has been accomplished in subtask operations such as torch guiding and seam tracking. One area where closed loop control has been in use for some time is the electrode/weld-pool separation by arc voltage feedback in GTA welding. Arc voltage control (AVC) is also used in Gas Metal Arc (GMA) welding to fix the distance of the consumable electrode to the plate. These examples of closed-loop control do not, however, effect control of the weld characteristics. Successful closed-loop control of weld variables has been accomplished for very specialized applications [1.2, 1.3] but is still in the initial stages of development. Closed-loop control of the weld itself is a potentially effective way to improve quality and productivity and may pose advantages over improvements which could be achieved by requiring tighter tolerances on the preparation, post-treatment or material composition itself. The research performed under this contract is an initial step toward achieving closed loop weld control and a first step in developing and evaluating this approach.

One significant activity has been to formulate a unified strategy to achieve closed-loop control, so a description of our overall approach to the weld control problem is first given. This is followed by a summary of the main accomplishments of our work, which are in the following areas:

(1) Plasma Jet Phenomena in Welding Arcs;

(2) Weld Geometry Control;

(3) Weld Puddle Geometry; and

(4) Arc Current Regulation.

2. M.I.T. Approach to Welding Automation

The control strategy which has been adopted in this work, is to decouple and separately regulate key determinants of a "good" weld. For example, independent control would be exercised on weld bead top and bottom width and on local temperature distribution history with the goal of maintaining a specified strength, toughness and fatigue characteristic in the joint. The expectation is that closed-loop control will be more effective in reducing defects from many of the disturbances which now cause difficulties in welding. At the same time, we recognize that weld control is not likely to resolve all the difficulties and thus one goal of our efforts is to evaluate the potential gains by control against the gains which can be achieved by other means.

In the long term, welding automation will be achieved by a combination of changes in fabrication, joint geometry, materials, and material conditioning practices, as well as by the application of direct welding control. The level of sophistication of the controller will be determined by the economic balance between reduction of setup and repair costs versus the added capital and maintenance cost of a more sophisticated device. Finally it is important to recognize that the control research efforts must be supported by improved physical understanding of the welding process and that placing a process under control requires an integrated approach where control systems are developed in parallel with sensor development, process understanding, and welding equipment redesign.

Once the selection of the key determinants of a good weld has been made, closed-loop control requires four components:

a) An on-line technique for sensing each of the variables to be controlled;

b) A physically based but computationally simple model relating the weld variables being controlled to the process imputs;

c) At least one control variable on the welding device for <u>each</u> weld variable being controlled; and

d) A control algorithm that combines the above components to provide independent output variable control.

While first generation closed-loop welding control systems will not require advances in the state-of-the-art knowledge of control theory, this does not imply that the development of the control system is a minor step consisting of "hooking-up a computer." Thus, the sensors, models and welding device control variables must be developed in parallel with the control system. Our approach is to close loops as early as possible and to advance in parallel the capabilities in areas a, b and c above. Further, we separate the problem of torch manipulation, i.e. welding robotics, from the closed-loop control of the weld itself. In the former, the purpose of the manipulator control system is to control where the torch moves rather than to directly control the properties of the weld being produced. The weld control system must instruct (control) the manipulator on how to move to achieve the desired weld characteristics. The total system consists of several inner loop (or

subprocess) controllers all supervised by the master controller, as shown schematically in Fig. 2.1 .

We have confined our efforts to Gas Tungsten Arc Welding (GTAW) of the root pass of a multi-pass weld or to autogenous welds of modest thickness. Further, in this initial work we have considered control only of the weld geometry, rather than considering all aspects of weld quality. These limitations are not severe, as the root pass is the most critical stage of a multi-pass weld (even though the fill passes might take more of the time) and the successful application of control to the root pass should allow a relaxing of the fit-up and material tolerances. Autogenous GTA welds are of interest because for modest thickness materials the single pass may be sufficient. We have also limited our efforts primarily to geometry control. Appendix A discusses some issues of control within the large context of welding fabrication. Finally, it must be recognized that the general approach to weld control and many of the sensors and models can also be used as a starting point for control of other welding systems.

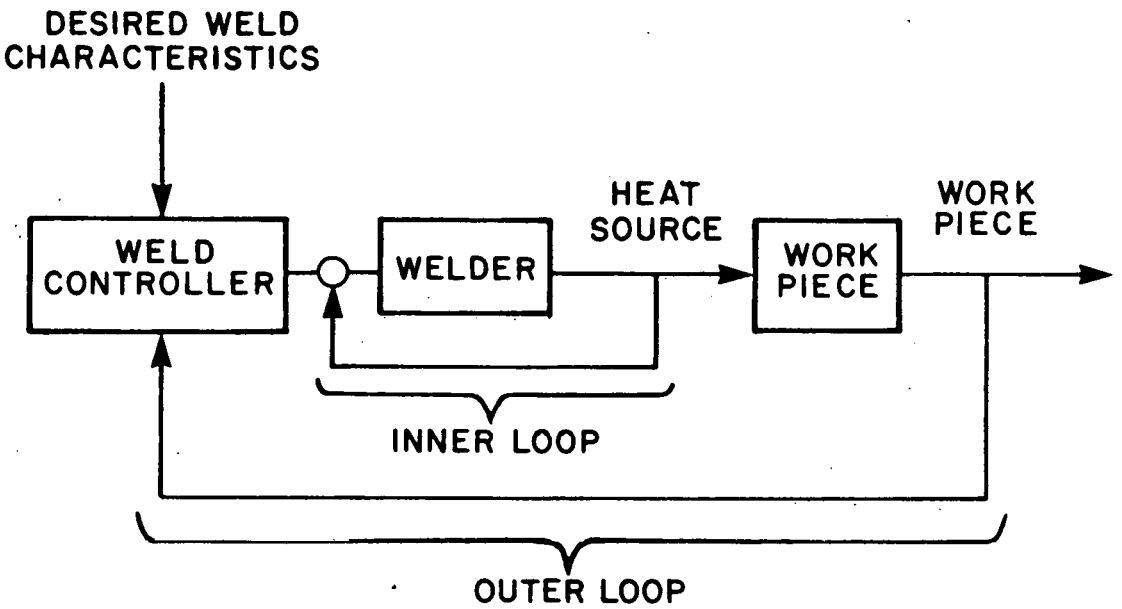

Figure 2.1 Schematic of Overall Control Strategy for Smart Welder.

3. Plasma Jets in Welding Arcs

Plasma jets originated by the electro-magnetic forces play an important role in the welding process by:

a) stabilizing the arc;

b) exerting pressure and shear forces on the weld pool; and

c) altering the metal transfer mode when a consumable electrode is used.

In these ways, the plasma jet behavior can be a significant factor in determining the quality of a weld. In the context of control, the strength and distribution of plasma jet force on the weld pool represent possible input variables which can be adjusted to keep an output variable, such as penetration, to a prescribed value. The success of current pulsing in GTA welding supports the importance of plasma jet forces. An understanding of the arc behavior is also important since the arc represents a source of diagnostic information, and signal processing of the voltage and current signals, for example, requires an understanding of the arc.

The first part of this section describes the main results of our study of the steady behavior of an arc between a GTAW torch and a flat plate anode. For steady flow conditions, we have developed a novel technique to measure the strength of the plasma jet and made measurements for a range of currents and electrode tip angles. Interpretive models were developed both for the tip region and for the developing jet region away from the tip. As discussed in the description of our overall approach, the efforts in modeling lean in the direction of physically based, but computationally simple, models. We have also explained the empirical results for the stiffness of arcs to external disturbances measured by other investigators in terms of the plasma jet phenomena.

The second part of this section discusses the results of our study of the unsteady behavior of the arc, in particular the response to strong and rapid changes in arc current. In addition, the time response of the arc to lateral deflections and other time varying disturbances reported have been measured.

3.1 Background and Theory

The basic structure of high pressure arcs is well established. The regions close to the anode and cathode are dominated by the interaction of the current with the wall and are generally areas with large departure from local thermodynamic equilibrium (LTE). In contrast, the region away from the electrodes, the positive column, is generally close to LTE and can be analyzed using the continuum fluid equations including the electromagnetic body forces and the bulk Joule heating of the gas. An arc, formed in an unbounded region, will expand to fill the region; therefore some sort of 'stabilization' of the arc must occur if the arc is to be confined to a finite size. A cooled wall, a forced swirl or axial flow of gas, natural convection currents around the arc, or fixed electrode size and short electrode separation are some ways arcs are stabilized. For the tip plane geometry the arc can be stabilized by the

self-induced plasma jet flow which results from the constriction of the current imposed by the tip electrode. Maecker [3.1], first explained this behavior in terms of the pinch effect, which produces a centerline pressure which is higher near the electrode than in the region away from the constriction. This explanation is incomplete and leads only to rough estimates of the plasma jet strength. The more exact formulation contained in other works is summarized below.

The main welding current establishes an azimuthal magnetic field which increases with distance from the center of the arc to the outer boundary. For a uniform distribution of current within the local arc radius R, the magnetic field is given as

$$B_\theta(r) = \frac{\mu I r}{2\pi R^2}$$

where μ is the magnetic permeability, r is the radial coordinate, and I is the total current through the arc. If the arc is constrained to keep a constant radius, the self magnetic field will result in a Lorentz force in the radial direction only. If the arc deviates from cylindrical shape, but maintains radial symmetry, the Lorentz force on the fluid will have both radial and axial components. In the absence of space charge effects, i.e. away from the electrodes, conservation of current requires

$$\frac{1}{r}\frac{\partial}{\partial r}(rJ_r) + \frac{\partial J_z}{\partial z} = 0$$

where $J_\theta = \partial J_\theta/\partial\theta = 0$ from symmetry considerations. The radial current density can be related to the axial change in arc radius, dR/dz, as

$$J_r = \frac{Ir}{\pi R^3}\frac{dR}{dz}$$

where $J_r(r = 0) = 0$ by symmetry and for convenience a uniform current distribution has been assumed. The body force is given as

$$\overline{J} \times \overline{B} = -\frac{\mu}{2}(I/\pi R^2)^2 \{r\,\hat{u}_r - \frac{r^2}{R}\frac{dR}{dz}\,\hat{u}_z\}$$

where $\hat{u}_r$ and $\hat{u}_z$ are unit vectors in the radial and axial directions. Both components of the force contribute to the circulation, with the radial force resulting in circulation through the arc center toward the plate and the axial force resulting in circulation in the opposite direction. Only the axial force leads to a net axial momentum on the fluid, as can easily be established by considering a cylindrical control volume around part of the arc. The total axial force on the plasma in the expanding current channel is evaluated by integrating the body force over the volume of interest and yields

$$F_z = M_0 = \frac{\mu I^2}{4\pi}\ln(R_2/R_1) \qquad (1.1)$$

where R_1 and R_2 are the arc radii at the initial and final stations of interest. The magnitude of the force is independent of the precise variation of arc radius with axial distance as long as the shape of the current distribution remains the same. When the fluid is turned at the plate the jet axial momentum is converted to a force on the plate; this force is in addition to the force exerted by the pinch effect. The total force on the plate becomes

$$F_{plate} = F_{mom} + F_{press} = \frac{\mu I^2}{8\pi} [1 + 2\ell n (R_2/R_1)]$$

3.1.1 Effect of Tip Angle

If the radius of the arc in the fully expanded region and the current density at the cathode are not strongly affected by the tip angle, a simple expression can be derived to relate the momentum imparted to the fluid to the tip angle of the electode, at least for constant arc current. For fixed current, a constant cathode current density implies that the cathode surface area A_c ($=I/J_{cathode}$) should remain fixed as the tip angle varies; thus the effective arc radius at the electrode, D_e, is related to the tip angle, α, as by

$$D_e = \sqrt{4 \sin \alpha \, A_c/\pi}$$

The flux of momentum can then be calculated as

$$M_o = \frac{\mu I^2}{4\pi} [\ell n \sqrt{\pi D_c^2/4A_c} - \ell n \sqrt{\sin \alpha}\,] \qquad (1.2)$$

where D_c is the diameter of the arc away from the tip region.

3.1.2 Deflection of the Arc by a Transverse Magnetic Field

If an external magnetic field is established in the transverse direction, the arc will be deflected. In the tip region, where most of the expansion of the current channel occurs, the arc is directed by the electrode and the deflection should be small. In the region away from the tip the momentum of the fluid is roughly constant in the absence of the external field and since there is no work done by the magnetic field on the plasma (the force is always perpendicular to the motion of the plasma) the momentum of the fluid must remain constant. The result is that the plasma path assumes a trajectory of a circle with radius R_c which can be found from $M_o = B_o I R_c$, where B_o is the strength of the applied magnetic field. If the radius of curvature is large and the arc remains tangent to the electrode at the tip, the radial deflection of the arc at a distance h from the electrode is given as

$$d = Ih^2 B_o/2/M_o \qquad (1.3)$$

where an approximate expression for the radius of curvature has been used.

The relationship of plasma jet phenomena to the stiffness of the arc to resist deflection from external magnetic fields is clearly established by

Eqn 3. If the simple expression for plasma jet momentum is used, the deflection can be expressed as

$$d = \frac{B_o \, 2\pi h^2}{I \, \mu \, \ell n(R_2/R_1)}$$

Assuming that the arc expansion ratio is roughly constant as the current is changed, the formula indicates that the arc stiffness ($=d/B_o$) should vary as the inverse of the arc current. The increase in stiffness gained from reduced tip angle can be determined by use of Eqn 2. Other techniques to increase plasma jet momentum at fixed current will also lead to increased stiffness.

3.1.3 Behavior of the Arc After the Initial Expansion Region

While the most critical region to model is the region near the tip where most of the momentum is imparted to the fluid, it is also of interest to model the development of the plasma jet downstream of this region. A simple jet development model was constructed; more complex models have been developed [3.2], but it seems hardly necessary if the near tip region is not to be modeled. The present model considers the development from the end of the main expansion region, by assuming simple velocity and temperature distributions at each axial location in the conservation equations for mass, momentum and energy and in the appropriate Ohm's Law equation.

As shown in Fig. 3.1, the arc is taken to consist of an inner core of uniform temperature and velocity. In the outer region the gas temperature declines to room temperature and the velocity is taken equal to the shield gas velocity. The inner core entrains fluid from the outer core and thereby increases in radius and slows down with axial distance. The gas is assumed to behave as an ideal gas and measured data is used to describe the variation of electrical conductivity, radiation loss and thermal conductivity with temperature.

Equation for Axial Growth of Jet. The entrainment of mass into the inner core is taken to be proportional to the velocity and the jet surface area; conservation of mass can then be expressed as

$$\frac{d\dot{m}_c}{dz} = \frac{d}{dz}\left[\pi\gamma^2 \, U_c(P/RT_c)\right] = 2\pi\gamma \, U_c(P/RT_c)\alpha \qquad (1.4)$$

where γ is the inner core radius, the subscript c denotes core, α is the entrainment coefficient, T, U, and P are the temperature, velocity and pressure respectively and R is the gas constant. Since the momentum is assumed to be transferred to the gas upstream of the region of interest, conservation of momentum flux for the core yields

$$\frac{dM_o}{dz} = \frac{d}{dz}\left[\pi\gamma^2 \, U_c^2 \, (P/RT_c)\right] = 0 \qquad (1.5)$$

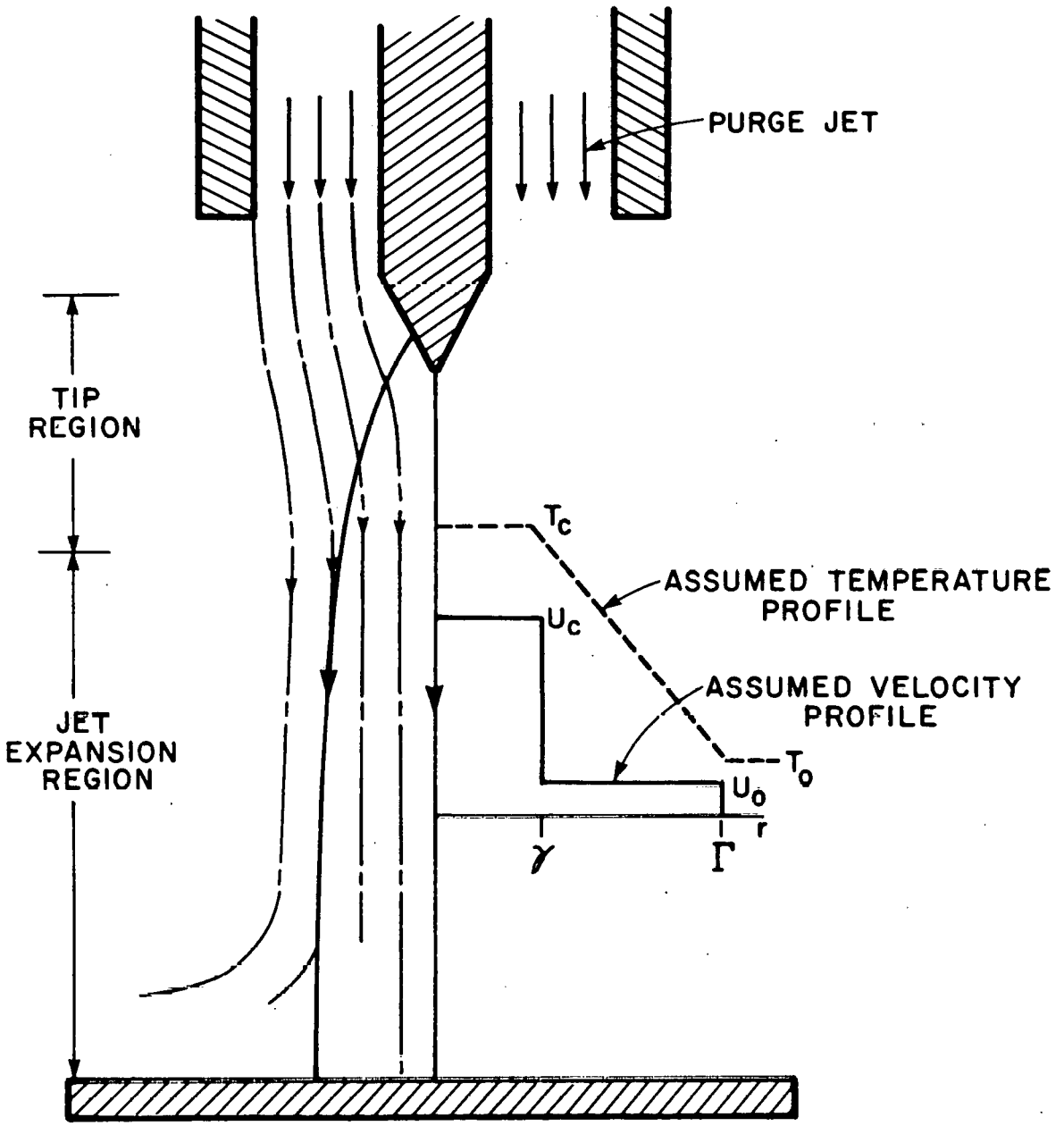

Figure 3.1 Sketch of Tip-Plane Configuration Showing the Assumed Profile Shapes for the Developing Jet Model and the Flow Pattern in the Tip Region.

The conservation equation for the inner core balances the enthalpy flux against Joule dissipation, heat conduction and radiation loss and can be written as

$$\frac{d\dot{H}_c}{dz} - c_p T_c \frac{d\dot{m}_c}{dz} = \sigma_c E^2 - 2\pi\gamma\ \lambda_c \frac{(T_c - T_o)}{\Gamma - \gamma} - \dot{q}'_{rad} \tag{1.6a}$$

with

$$\dot{H}_c = \pi\gamma^2\ U_c\ (Pc_p/R) \tag{1.6b}$$

and where λ_c is the thermal conductivity, E is the electric field, σ_c is the electrical conductivity, T_o is the temperature of the incoming shield gas, c_p the specific heat and $\dot{q}_{rad}$ is the heat lost from the core per unit length by radiation. The radiation loss is evaluated from the volumetric loss, $\dot{q}'''_{loss}$ assuming that gas is optically thin thus

$$\dot{q}'_{rad} = \dot{q}'''_{rad}(T_c)\ \pi\gamma^2$$

where $\dot{q}_{rad}$ is supplied by the experimental results of Emmons.[3.3] The energy balance on the entire arc can be written as

$$\frac{d\dot{H}_t}{dz} - c_p\ T_o \frac{d\dot{m}}{dz} = EI - \dot{q}'_{rad} \tag{1.7a}$$

with

$$\dot{H}_t = \pi(\Gamma^2 - \gamma^2)\ U_o\ (Pc_p/R) + \pi\gamma^2\ U_c(Pc_p/R) \tag{1.7b}$$

where U_o is the velocity of the purge gas. The second term on the left hand side of Eqn (1.7a) can be neglected since $T_o \ll T_c$. The total radiation loss per unit length is taken equal to the loss from the core. The final equation required is Ohm's law which relates the electric field to the current as

$$E = \frac{I/\pi\Gamma^2}{\langle\sigma\rangle} \tag{1.8}$$

where $\langle\sigma\rangle$ is the average conductivity over the arc cross-section. The electrical conductivity is a function of temperature and taken to be

$$\sigma = AT^B \tag{1.9}$$

where A and B are constants for a particular gas mixture.

Eqns 1.4, 1.5, 1.6a,b, 1.7ab and 8 represent 5 equations in the 5 unknowns; γ, Γ, U_c, T_c and E, (H_c, M_o and H_t are intermediate quantities which are easily eliminated for the equations) which can be integrated in z for a given arc current.

Initial Conditions. The conditions at the end of the current expansion region are partly determined by experimental data. The momentum flux is taken as

$$M_o = \pi\gamma^2 U_c^2 (P/RT_c)_{z=o} = [1 + 2\ell n(R_2/R_1)]\mu I^2/8\pi$$

where the experimental value of $[1 + 2\ell n(R_2/R_1)]$ is used. The results were found to be insensitive to the choice of the initial outer region radius, so it was assumed to be $\Gamma(z=0)=2\gamma(z=0)$. A third condition was obtained by assuming that the temperature T_o is a maximum at the end of the current expansion region, which results in using Eqn 6a in the relation

$$\sigma(T_c) E^2 = \dot{q}'''_{rad}(T_c)\pi\gamma^2 + 2\pi\lambda_c\gamma \frac{T_c - T_o}{\Gamma - \gamma}$$

at z=0. Ohm's law, evaluated at z=0 represents an additional equation. The final initial condition is obtained by choosing the initial velocity U_c to give the proper arc voltage gradient for a current of 100 amperes; for argon arcs this field is 8 V/cm.[3.4]. For other currents, the initial velocity is assumed to vary linearly from this value.

Entrainment Coefficient. For a turbulent jet an entrainment coefficient of ~0.1 is typical. However, for the somewhat low currents considered here the jet Reynolds number is ~10-100 and the flow can be expected to be laminar. For a lamanar jet the entrainment rate is

$$\frac{\dot{dm}}{dz} = 8\pi\mu$$

rather than proportional to $2\pi\Gamma U_c\ell$ as has been assumed. Nevertheless, reasonable results can be found by taking the formulation of Eqn (1.4) with $\alpha = 0.055$.

Calculated Results. The The axial variation of the quantities for a 100 A are shown in Fig. 3.2 As can be seen, the inner core grows linearly with axial distance, while the outer core grows more rapidly near the start. The predicted variation with total current of voltage drop (away from the electrodes) is shown in Fig. 3.3 and indicates increase in voltage from 7 volts at 40 amperes to 10 volts at 240 amperes.

3.1.4 Modeling of Transient Response

As will be shown in the experimental section, rapid increases in the arc current result in the formation of a vortex structure that propagates from the tip region. This type of behavior has been observed for starting hydrodynamic jets by Witze [3.5.] The analysis of Abramovich [3.6] is used to consider the response of the plasma jet to a change from a very low current (~10 Amperes) to a high level. The assumed structure of the jet transient is shown in Fig. 3.4. A spherical vortex of radius R, moves away from the tip. The vortex mass increases due to entrainment of mass from the jet forming behind

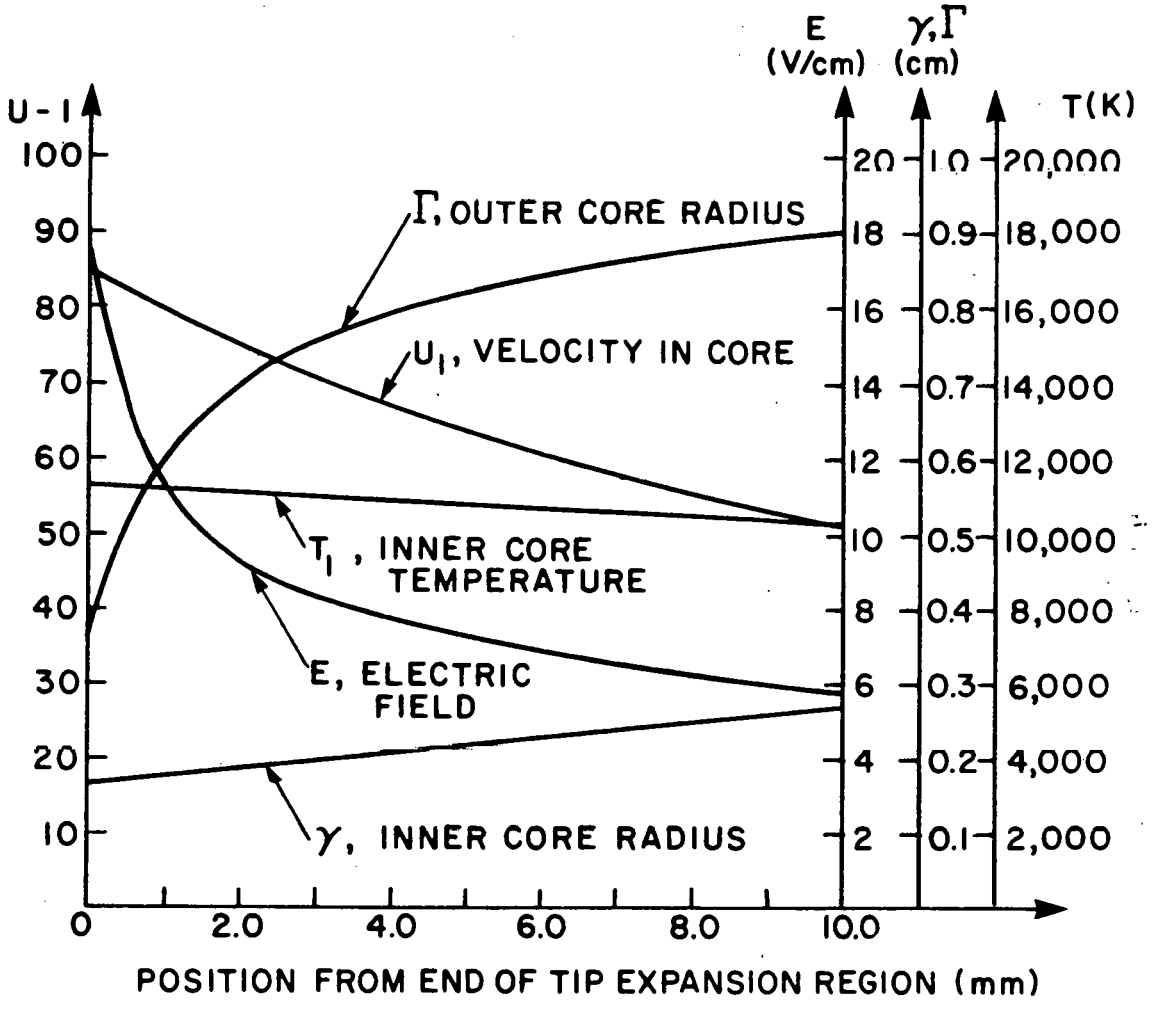

Figure 3.2 Solution for a 100 Amps Arc.

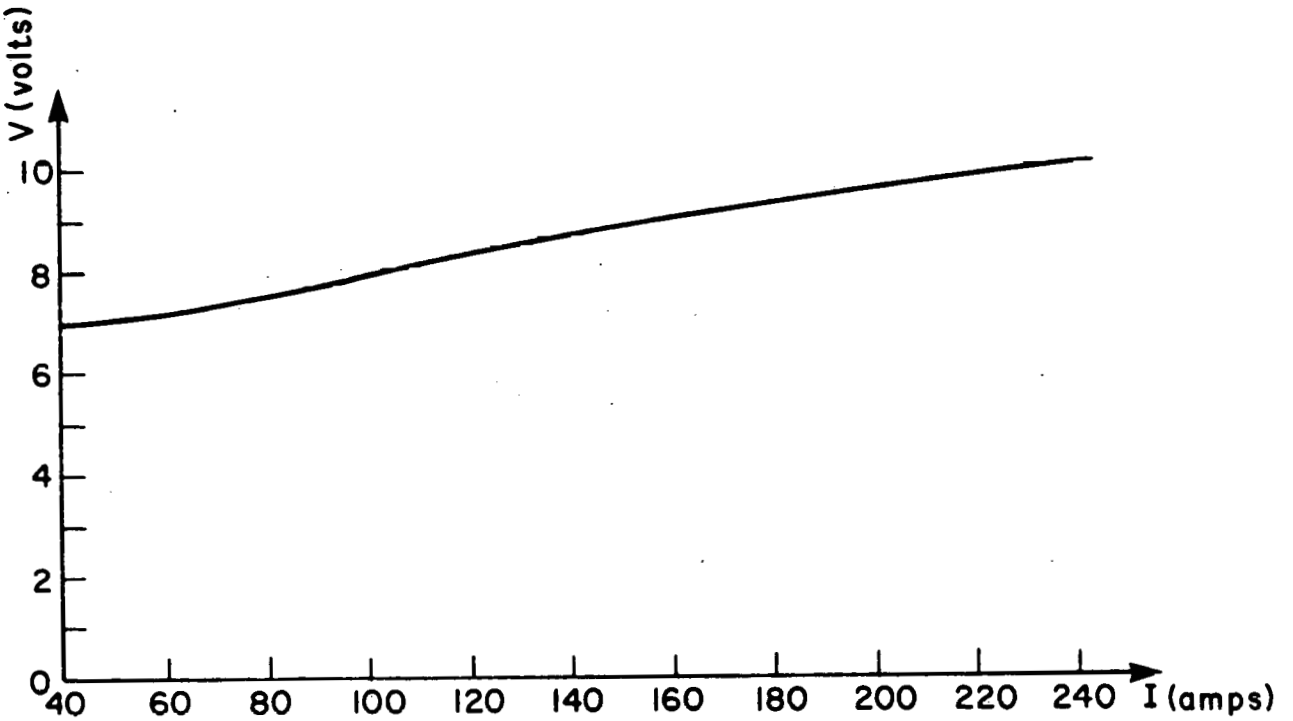

Figure 3.3 Voltage Drop Through the Arc Versus Current.

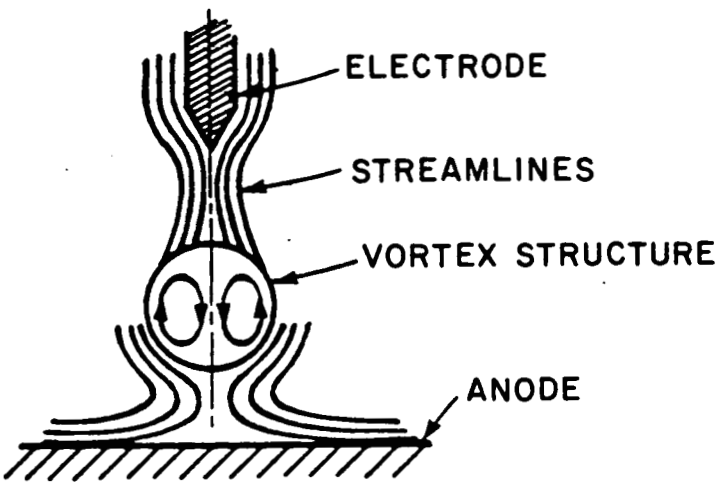

Figure 3.4 Vortex Structure Convected Away from the Tip.

it; the vortex is pushed through the still air by the jet behind it. Following Solon, equations can be developed for the time variation of the volume of the vortex and axial location of the vortex. Entrainment to the vortex is assumed to come entirely from the jet, and is taken as

$$\frac{dV}{dt} = \pi\gamma^2 (U_c - U)$$

where V is the vortex volume, U is the speed of the rear of the vortex, γ and U_c are the radius and velocity of the steady jet growing behind the vortex and are taken from the steady solution described in the previous section. The momentum balance for the vortex includes the momentum flux from the jet, viscous drag and the inertia imposed by the need to move fluid out of the path of the vortex. The latter term is determined from the potential flow solution discussed by Milne-Thompson [3.7]. In the present case, some assumption about the density of the volume displaced must be made and in the results shown below the density is evaluated at the average of the arc temperature and the ambient gas temperatures. The drag force is evaluated from data of laminar flow around a sphere [3.8]. The final form of the momentum equation is

$$\frac{dU}{dt} = \frac{1}{V}\left\{\frac{(U_c-U)U_c\pi\gamma^2}{(1+\rho_{eff}/\rho_c)} - U\frac{dV}{dt} - 1/2\,\frac{U^2}{(1+\rho_{eff}/\rho_c)}\,\frac{13\ \pi R^2}{(2RU\rho_c/\mu)^{1/2}}\right\}$$

The position of the rear of the vortex can be found as $dz/dt = U$ and the three equations numerically integrated (using the steady plasma jet solution) to find the position of the vortex.

The result is shown in Fig. 3.5 for a step change to a current of 200 amps. As can be seen the speed is roughly constant and equal to ~50m/sec for this case.

3.2 Experimental Apparatus and Procedure

The experimental measurements of the plasma jet momentum were conducted in a stationary torch setup shown schematically in Fig. 3.6. A conventional GTA torch was used, typically with argon shielding gas, to create the arc plasma with a water-cooled copper plate used as the anode. The rig was designed to allow full optical access to the welding region, and to provide for easy modification and interfacing with diagnostic instrumentation.

A GTAW torch (Airco Heliweld H20-C) with a 3/32" diameter, 2% thoriated tungsten electrode was used in all the experiments. The tip was ground to a conical shape and a shadow of the tip projected on a screen to accurately measure the tip angle. A large diameter cable was connected directly to the electrical contact in the torch head, thus avoiding the use of the normal, high impedence, cable which runs the length of the water-cooling hose. This

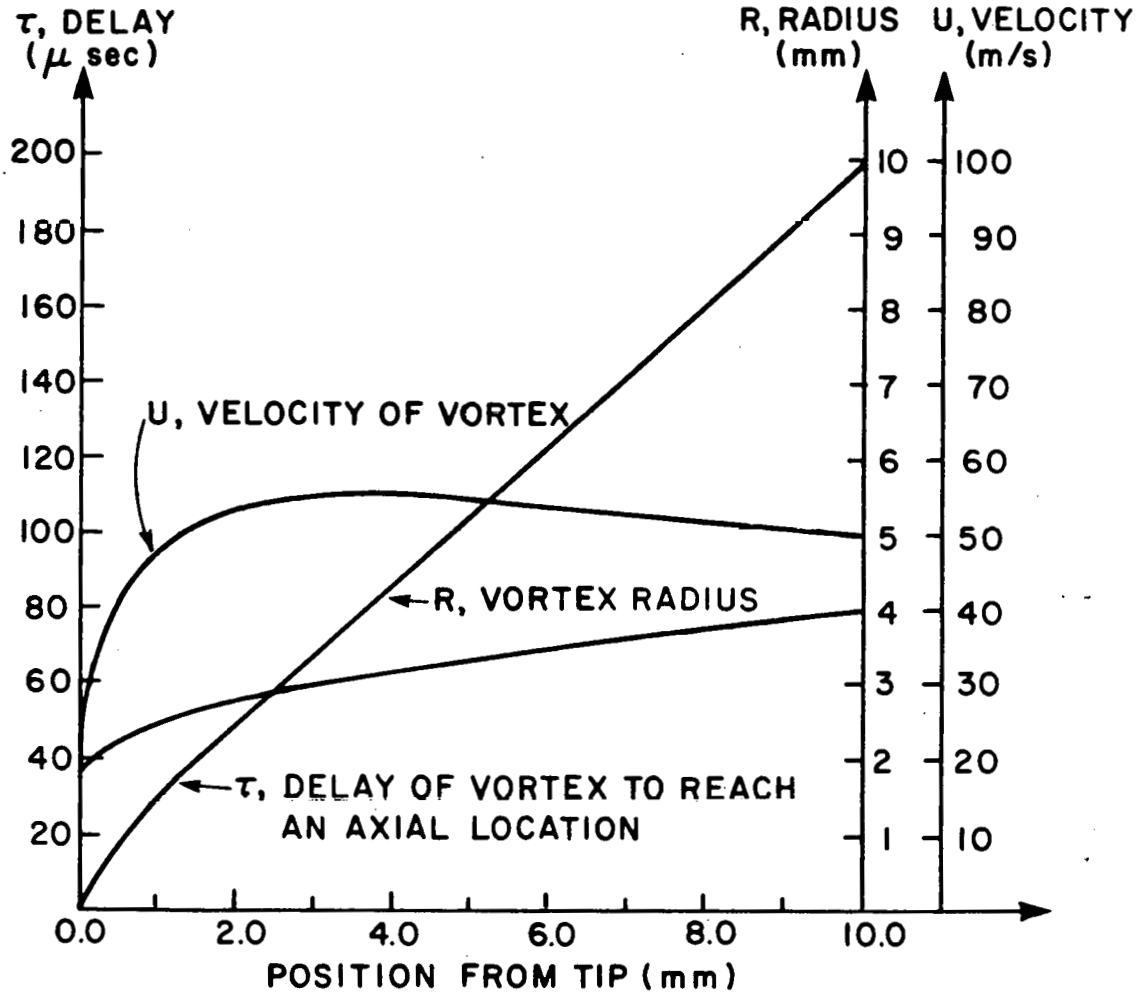

Figure 3.5 Response of an Arc to a 200 A Step Change in Current

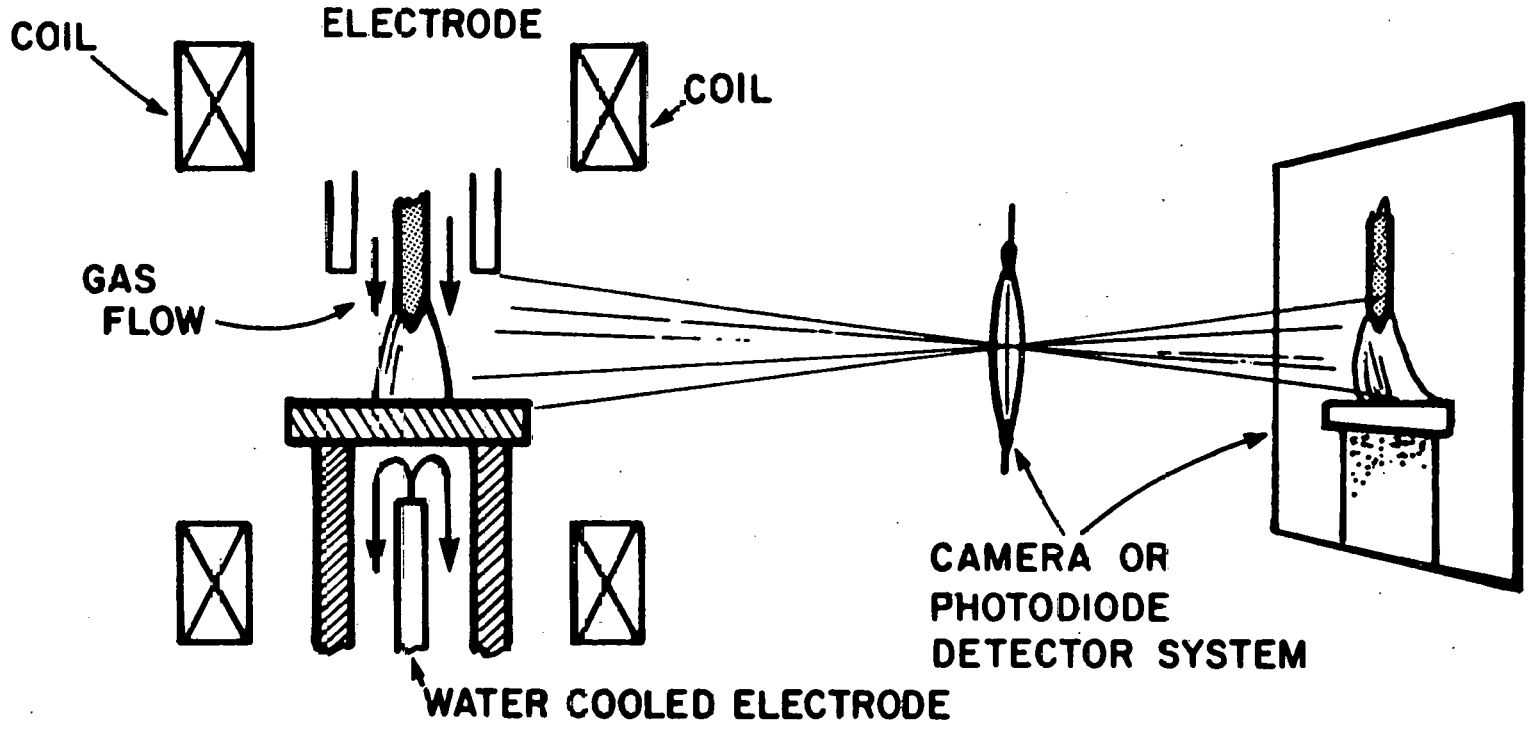

Figure 3.6 Schematic Showing Arc Deflection Technique.

was necessary for the high frequency runs to be conducted properly. A 3/8" diameter alumina nozzle was used to direct the welding quality argon purge flow, which was fixed at 18 cfh. The workpiece was made of 1/4 inch Oxygen-Free-High-Conductivity copper, silver-soldered to a stainless-steel stem. The stagnation flow cooling water configuration was used to prevent film boiling at the high local heat transfer rates. The top surface of the electrode was remachined or replaced whenever it became pitted.

A standard 3-phase rectified power supply (Airco CV-450) capable of providing 450 amps at 38 volts was used as the main power source; the high current option of the supply was used to avoid the inductance introduced in the low current circuit. A unique current controller designed and constructed, to our specifications, by Alexander Kusko, Inc. [3.9] was used. This transistor based device places the welding current under tight control and allows variation of welding current over its full range (0-300 amps) with a bandwidth greater than 20 kHz. In the transient studies, the device was used to impose rapid changes in arc current; for example the current was increased by 60 amperes with a rise time of 15 micro-seconds. The current from the device can be controlled directly by a computer, but in these experiments a signal generator was used to define the output current from the regulator.

The magnetic field for the deflection experiments was provided by a pair of coils set up in the Helmholtz configuration, which yields a uniform field. A maximum magnetic field strength of 100 Gauss was possible with the coils. The magnetic field at various currents was measured using a Gaussmeter and the resulting calibration curve used to determine the magnetic field from the measured magnet current.

In addition to arc voltage and arc current measurements, several optical diagnostics were used. For the steady-state plasma jet measurements a charge coupled photo diode (CCPD) linear array, manufactured by Reticon, was used to measure the light emission intensity and thereby determine the distance the arc was deflected by the magnetic field . A simple lense arrangement was used to project the arc on the diode array (see Fig. 3.6); no spectral filtering was performed. Transient measurements were made using a single photo-diode (EG&G model SGD-100A), which allowed fast response measurements for a single location in the arc. A lense was used such that the diode accepted light from a narrow pencil through the arc with a diameter of 200 microns; no spectral filtering was performed. The output of the CCPD and the single diode were recorded using an oscilloscope.

3.3 Experimental Results

3.3.1 Steady Flow Momentum Flux

The momentum flux of the plasma jet was determined by measuring the deflection of the arc for a known value of magnetic field. As shown in Fig. 3.7 the CCPD array was placed a distance h from the image of the tip of the electrode and the radiation intensity profile determined from the diode array. Although a measurement of the deflection at a single combination of magnetic field strength and separation distance is sufficient to determine the momentum flux at a value of arc current, in the present investigation the momentum was

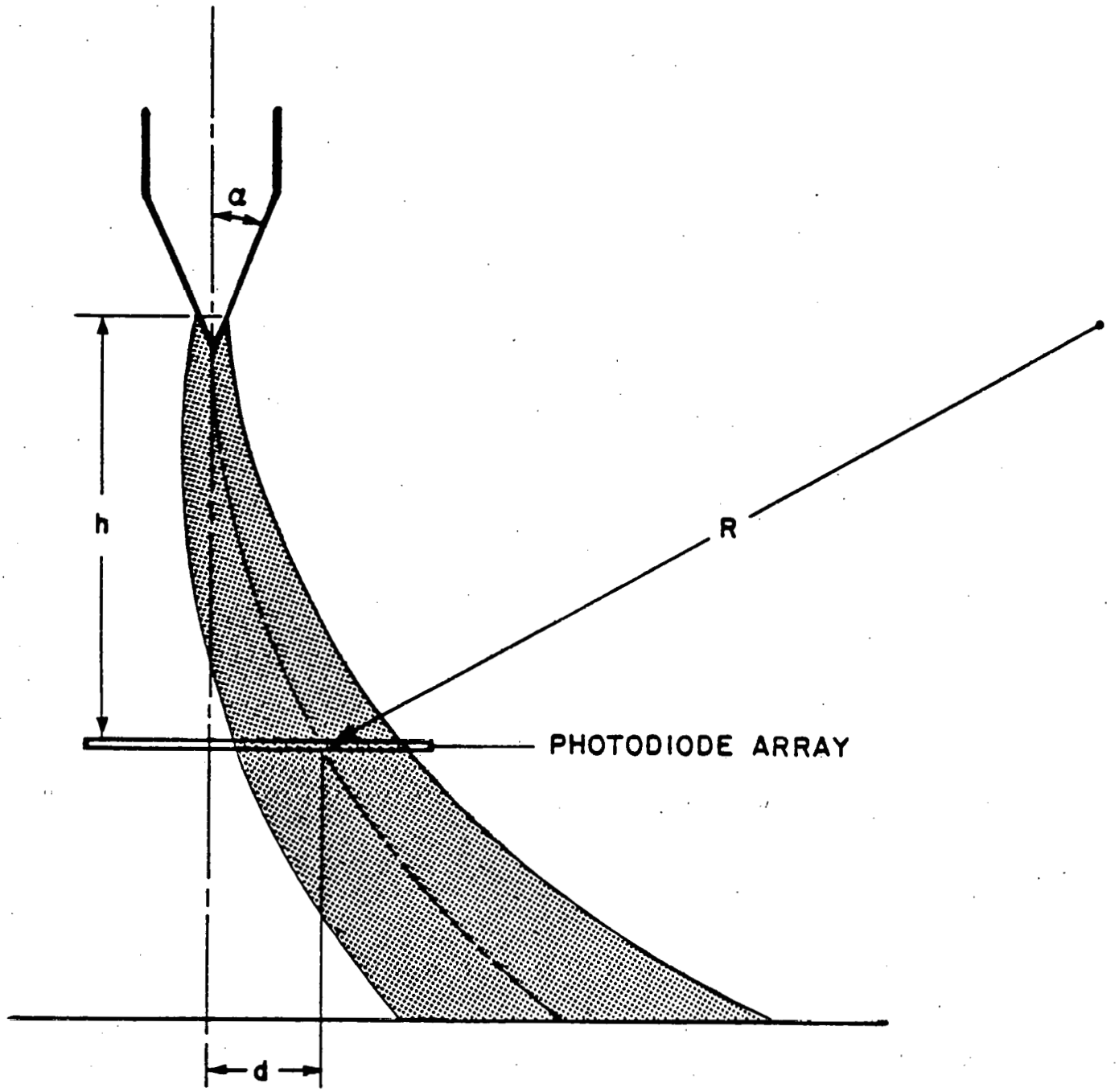

Figure 3.7 Position of Array With Respect to Arc.

determined from measurements over a range of magnetic field and separation distance. A typical set of results are shown in Fig. 3.8 where the deflection of an arc carrying 100 amperes is plotted as a function of magnetic field strength for several separation distances. The magnetic field strength was limited to 10 Gauss to keep the deflection low and keep the distortion of the arc to a minimum. The scatter of the results from the many redundant measurements was typically 10%.

The variation of momentum flux with current for a torch with a tip angle of 32.8° is shown in Fig. 3.9. For comparison, the force from the radial pressure distribution is shown and can be seen to be approximately a factor of 3 lower, at least for the tip angle of these experiments. The effective expansion ratio, R_2/R_1, is approximately 4.5. The variation of momentum flux with tip angle was also measured. The results for an arc current of 100 amps are displayed in Fig. 3.10 and show the expected trend of increased momentum at sharper angles. The results for angles from 32 to 60 degrees are consistent with the simple theory developed earlier and indicate a cathode current density of ~100 A/mm^2. For the larger angles the momentum drops faster than the simple model predicts indicating that either the cathode current density is decreasing or that some fluid mechanical effects have become important.

3.3.2 Transient Arc Characteristics

The response of voltage and radiation emission intensity from the arc to a rapid increase and to a rapid decrease in arc current has also been measured. The expected result was that the emission intensity would first increase in response to the excess Joule dissipation and then, as the fluid was replaced by fluid which had transmitted through the tip region after the current change, the emission intensity would again change. Since the jet velocity decreases with radius, it was expected that the second part of the response would arrive later for the regions farther from the centerline. At the centerline the propagation speed should be equal to the centerline velocity which for an arc current of 100 amps should be about 100 to 150 m/sec [3.10] In contrast, the measured response of the emission intensity to a rapid increase in current showed a delay consistent with a speed of about 50 m/sec at a current of 100 amps and that the delay was not a function of distance from the arc centerline. These results are shown in Fig. 3.11a and 3.11b. Since the measured response was similar to the observations of hydrodynamic starting jets, the model discussed earlier was developed to give an approximate speed of the vortex. The predicted propagation velocity by that model was in rough agreement with the measured speed. Further, the flat distribution is consistent with the vortex propagation.

3.4 Summary and Application to Welding Control

The results presented above clearly show the need to consider hydrodynamic effects when modeling the steady and unsteady behavior of welding arcs. A non-intrusive technique to measure the momentum of the plasma jet has been developed and implemented. The arc exerts force on the plate both from the conventional pinch pressure, but also from the turning of the net momentum applied to the gas from the expansion of the current channel in the vicinity of the tip. For the present experiments, the contribution to the force from

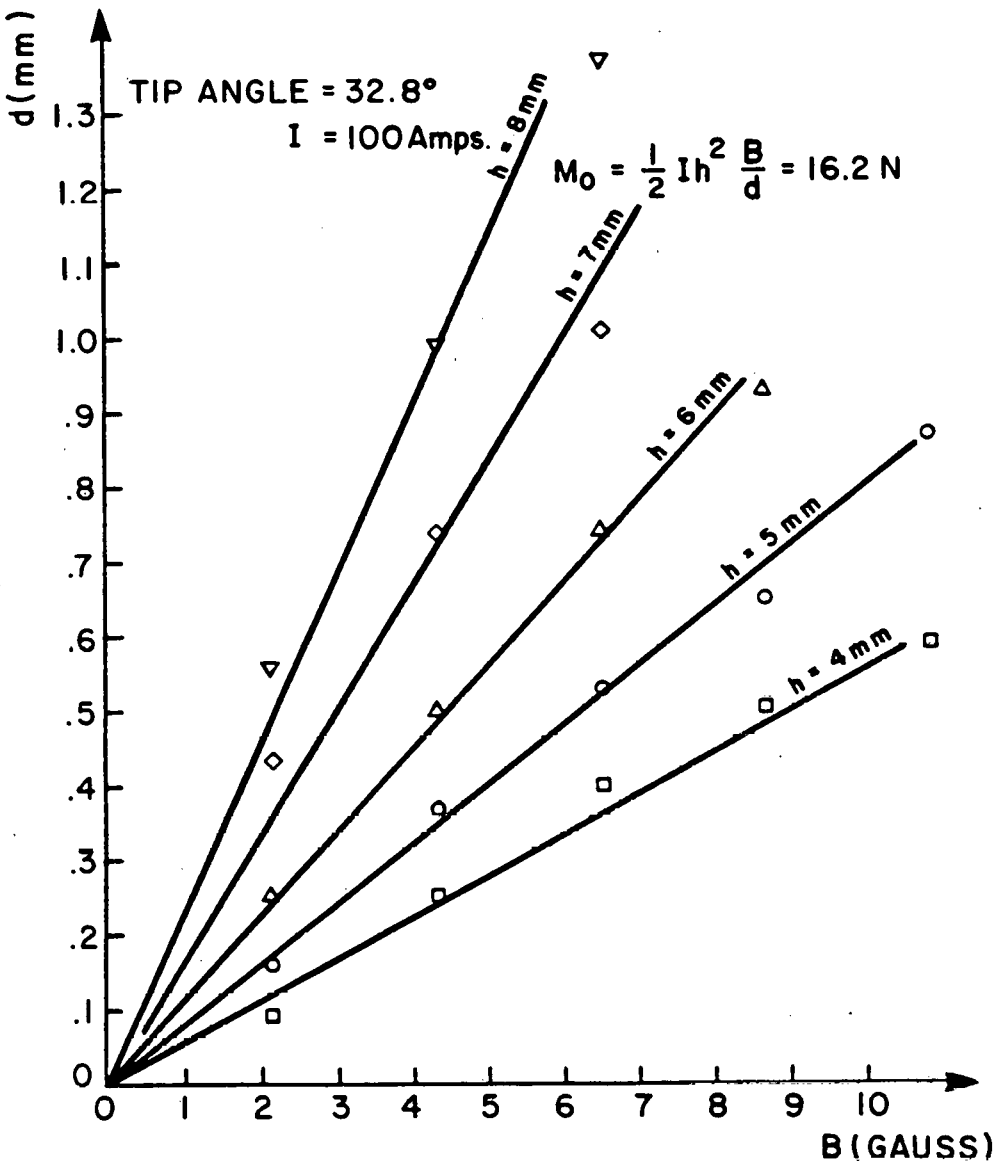

Figure 3.8 Arc Displacement as a Function of Magnetic Field.

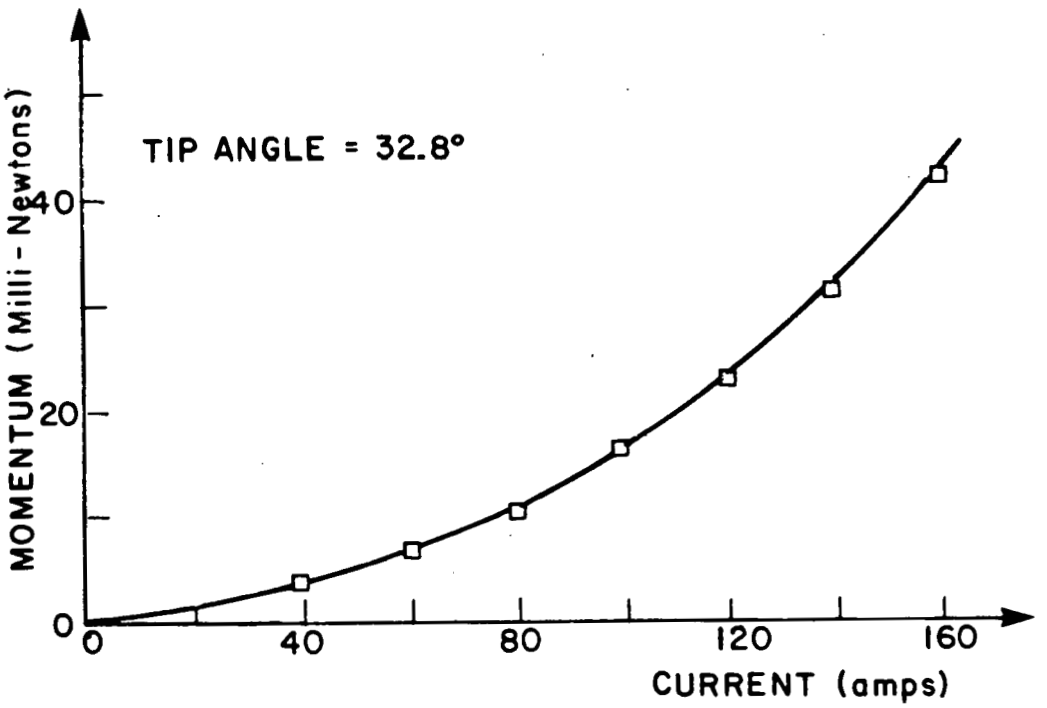

Figure 3.9 Flux of Momentum as a Function of Current.

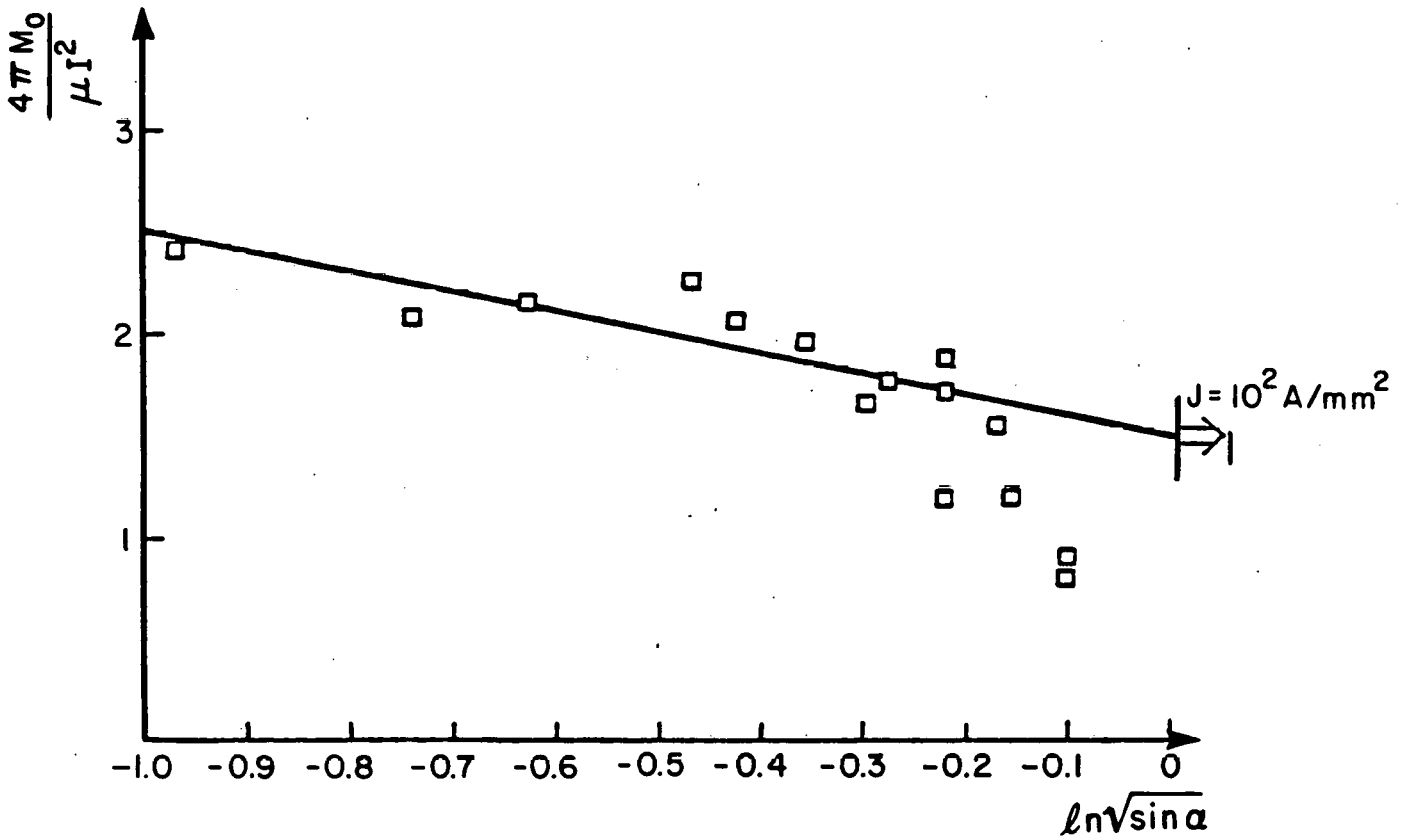

Figure 3.10 Predicted and Measured Variation of Plasma Jet Momentum with Tip Angle for An Arc Current of 100 Amps.

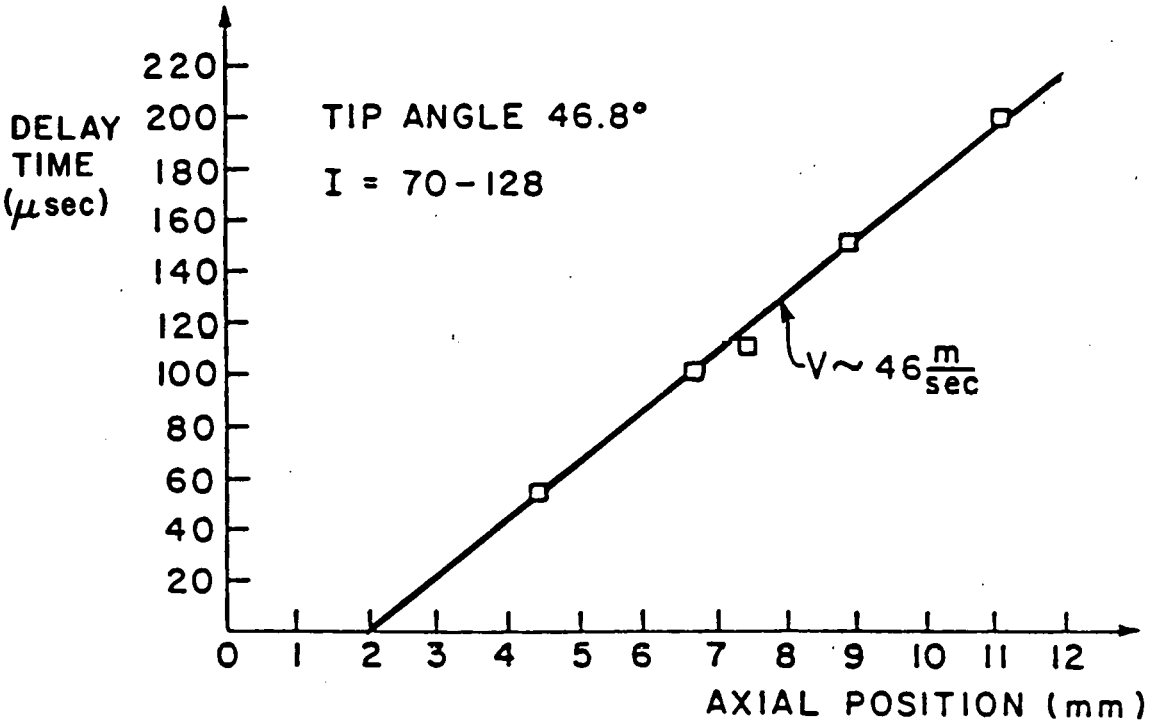

Figure 3.11a Wave Front Delay as a Function of Distance from the Electrode Tip.

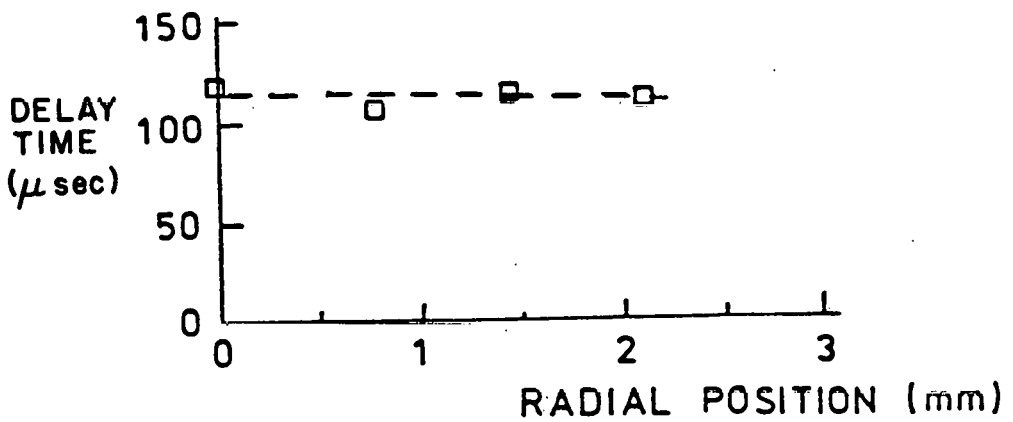

Figure 3.11b Wave Front Delay as a Function of Radial Position. Diode is Located 7.mm From Tip.

the momentum was ~2 times that from the pinch pressure. The source and numerical value of the stiffness of the arc to deflection by external magnetic fields (or by external fluid flows) is explained in terms of the momentum flux of the plasma jet. When the arc was subjected to a near step increase in arc current, a vortex structure was found to propagate from the tip; for long arcs, the propagation of the vortex is the limiting factor in reaching the new steady-state.

While some conditions of the present work were different from actual welding conditions (the arc was longer, the planar geometry somewhat unrealistic), the present work can be used to make some comments on the welding process, in particular upon ways to effect control of the weld geometry. To the extent that the plasma jet force controls the motion of the weld pool, modulation of the plasma jet momentum can effect changes in the weld geometry. In particular, the plasma jet momentum varies as

$$M_o \quad \langle I^2 \rangle$$

for modest frequencies of oscillation. In contrast, the heat input at the anode varies closely to

$$Q \sim \langle I \rangle$$

since the electron fall at the anode is not a strong function of current. Therefore, current pulsing at speeds higher than the puddle thermal time constant may result in increased weld penetration for a fixed weld pool width. Since weld geometry control is one important aspect of maintaining high weld quality, the ability to separately control width and penetration is extremely important.

4. Weld Geometry Control

4.1. Introduction and Background

Three major determinants of weld quality are: weld pool geometry, metallurgical properties of the weld metal, and heat effect on the base metal. Although a complete in-process control system would account for all three, our efforts in this research project have concentrated on weld geometry, since this is the primary indicator of integrity.

In the molten state, weld geometry can be defined by the maximum width and penetration of the puddle at any instant, and it is these dimensions that we wish to place under active control. By having closed-loop geometry control, the resulting welding device will produce welds of a consistent geometry that can be varied to suit the welding conditions and, most importantly, this consistency will be maintained despite variations in the welding environment. Clearly, any automated welding device must have these properties to produce welds successfully without supervision.

This is well illustrated by the example of autogenous GTA root pass welds on pipe, where complete melting of the root is required. The major problems are incomplete melting, which results in unfused metal and a crack initiation point, or burn though, where molten metal material detaches from the weldment and leaves a hole in the weld. Active geometry control applied here would eliminate these problems by commanding the welding device to melt only enough material to completely fuse the joint without risking a burn through, and then to maintain a specified backbead width.

The first step toward developing a full penetration geometry control system is to examine the physical phenomena that can be exploited to relate the weld geometry to measurable parameters. Katz [4.1] has investigated a method to sense the extent of penetration and even the puddle shape, in real-time using ultrasonic pulse echo techniques. The technique is based on the fact that the material density and the materials ability to sustain shear is changed at the metal-liquid interface. It has been shown experimentally that the ultrasonic reflections can be related to the size of the puddle in a stationary rod-like geometry where the puddle is made in one end of the rod and the ultrasound transducer is at the other end. However, the goal of two dimensional shape measurement has not yet been reached.

Vroman and Brandt [4.2] used a line scan camera to measure the width of the top side of a weld to allow closed-loop regulation of that variable. The width to depth ratio of a weld remains nearly constant under fixed welding conditions, as long as the puddle penetration is small compared to the thickness of the workpiece. Under these conditions, controlling the top weld width results in a regulated penetration. However, Vroman and Brandt experienced controller problems associated with pure delays introduced by their measurement technique and the true promise of this approach remains to be realized. This problem has been recently resolved by the on-electrode axis measurement technique developed by Richardson et al. [4.3]

Another approach involved sensing the back bead radiation. Nomura et al. [4.4] measured the infrared radiation from the back side of the weld for partial penetration submerged-arc welding, and succeeded in regulating the intensity of this radiation by varying the current. However, penetration and

back side thermal radiation are not simply related, and other factors such as weldment thickness and preheat can drastically change this relationship as was shown in their results.

Garlow [4.5] has used a single phototransistor to directly sense the back bead width of full penetration welds by measuring the amount of visible light radiated from the liquid surface. Since this is a single variable analog measurement, the bandwidth problems associated with scanned arrays are avoided. Also, this measurement method appears to be insensitive to material thickness and preheat, but it is sensitive to the emissivity of the materials being joined. Details of this work are include later in this Section.

4.2. The Puddle Impedance Technique

In this work we developed a method for sensing the extent of full penetration that did not require access to the back side of the weldment. The method takes advantage of the changes in mechanical behavior of the weld puddle that occur when the transition from partial to full penetration takes place.

As full penetration is reached, there is no longer any solid material to support the puddle and the weight of the puddle is supported mostly by surface tension. As the puddle moves vertically the angle of these forces changes providing a position-dependent vertical force, that is, a spring (see Fig. 4.1). The resulting mechanical impedance of this system determines the response of the puddle to periodic forces, and can be charaterized by the natural frequency and damping ratio of the puddle mass-surface tension system. This natural frequency will be shown to be related to the size of the puddle, and can be used to indirectly sense the back bead width.

The proposed measurement technique based on the impedance of the puddle involves exciting the puddle with a vertical force (originating, for example, from the torch plasma jet momentum), measuring the puddle motion, and then calculating and regulating the natural frequency. Once excited, the vertical position of the top surface of the weld must be measured. An attractive method to do so uses the fact that the puddle motion changes the arc length, which in turn changes the arc potential. Consequently, arc voltage measurement is sufficient and no additional instrumentation is needed. However, interpreting the arc voltage is very difficult, since there are many other factors influencing this potential, and this difficulty suggests that other methods of measuring puddle motion from the puddle surface may need to be studied. In the work described below both the arc potential method and a laser shadowing technique were used to measure puddle motion. Only the latter gave unequivocal results and this technique is not practical for on-line use since it requires access to the backside of the weld. However, we have had some encouraging preliminary results using the arc potential and with additional effort a practical system using only the arc potential should be achieved. The work described below represents a validation of the basic puddle impedance concepts upon which the final system development will be based.

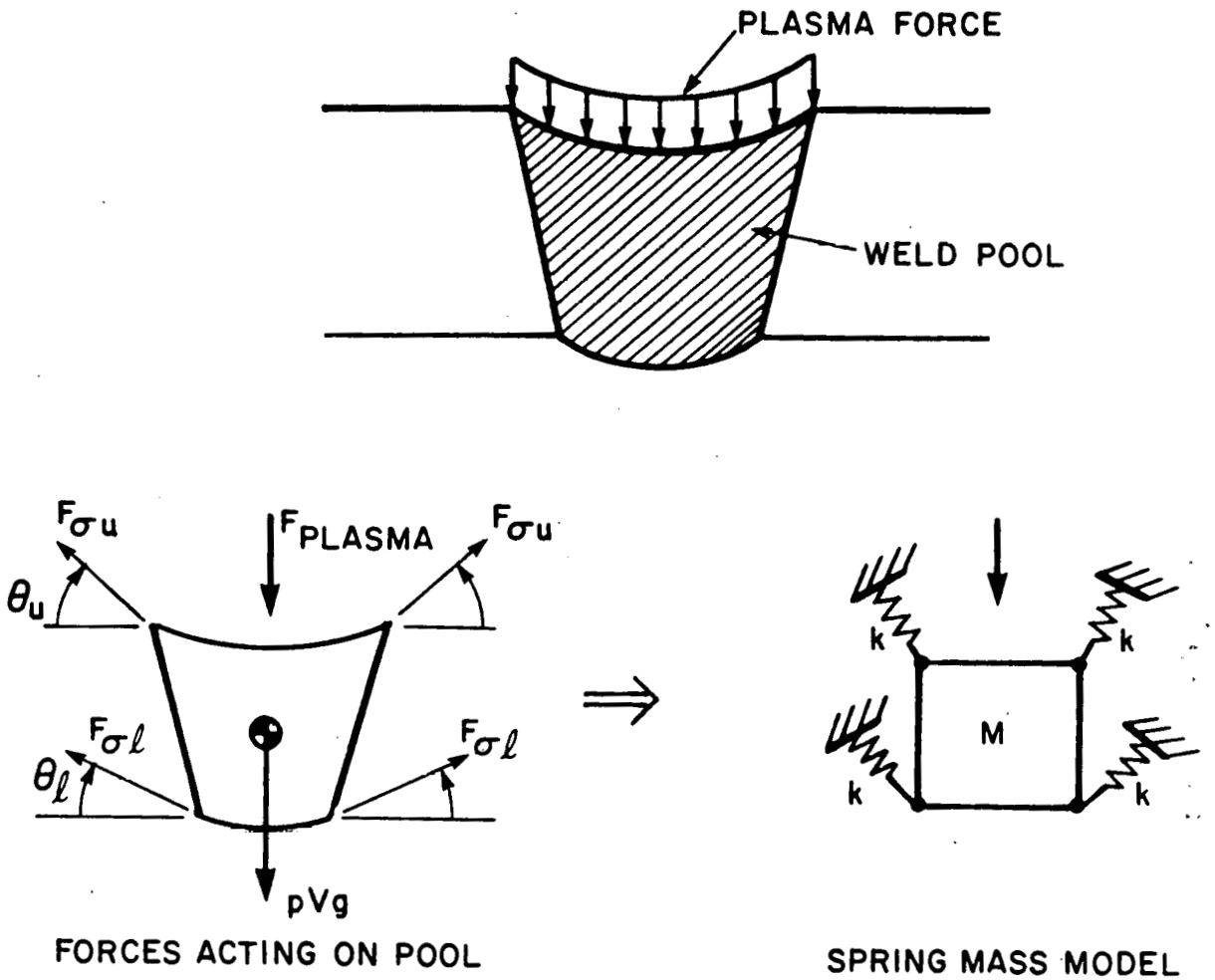

Figure 4.1 Model of a Completely Melted Weld Bead.

4.2.1. Theoretical Considerations

A theoretical analysis of the puddle motion for the simplified case of a stationary puddle having cylindrical shape was done using a lumped parameter approach (Zacksenhouse and Hardt [4.6]). The assumed cylindrical shape is somewhat similar to the actual shape of a stationary puddle at extensive full penetration. This shape, however, does not accurately describe either a stationary puddle at partial or slightly full penetration (the latter being defined as the case when the back bead radius is small compared to the top bead radius), or the puddle shape under a moving torch.

The natural frequency of the puddle surface motion was found to be

$$w_n = \frac{b_{oo}}{R}\sqrt{\frac{2N}{\rho h}} \qquad (4.1)$$

where N is the surface tension, ρ the liquid metal density, h the height of the puddle-cylinder, R is the radius of the cylinder and b_{oo} the first zero of J (z), the Bessel function of the first kind and order zero. It can thus be seen that the natural frequency will vary inversely with the puddle radius and as the square root of the material property descriptor N/ρ.

The expected natural frequencies can be calculated from the above equation using $\rho = 7.8 \times 10^{-6}$ kg/mm^3, N = 1 N/m, g = 9.8 m/s, $b_{oo} = 2.4$, and h = 2.5mm (the plate thickness used in the experiments). It was found that w_n is 40 Hz for R = 3mm (typical for continuous welds) and 20.4 Hz for R=6mm (typical for a stationary weld).

In a lumped parameter approach the puddle is modelled as a mass-spring system; hence, a second order transfer function relating output motion to input force can be defined. In the frequency domain such a system can be identified by a -40db per decade roll-off line on a log magnitude-log frequency plot.

4.2.2. Puddle Excitation

To measure a mechanical impedance the system has to be excited and its reaction measured and evaluated. As discussed in the previous Section, the pressure the arc exerts on the puddle is proportional to the square of the current. Thus by adding a sinusoidal AC component to the normal DC current level, the puddle can be excited at any desired frequency. However, because of the non-linear relationship between plasma force and torch current (as delineated in Section 3) the AC component should be small compared to the D.C. component of the current, preferably less than 10%, to achieve the linear characteristics necessary for the frequency response test.

4.2.3. Steady vs. Continuous Case

The model developed above was for a stationary puddle with a cylindrical shape. The actual shape of the puddle in a continuous weld is different. Furthermore the torch-puddle topology is different, and during a continuous weld the torch is not necessarily directly above the full penetration region. As a result, the motion resulting from the arc force may not be parallel to the torch and may instead have some inclination.

The experiments detailed next investigate the puddle impedance concept using a stationary puddle. Apart from the fundamental differences between a stationary and a continuous weld, there are some practical considerations that involve the evaluation of the experiments. With a stationary torch the level of the DC current used is much lower than the one used during a continuous weld. With continuous welds the current level is determined by the required heat input per length of weld, which is inversely related to the torch velocity, therefore high torch-velocities require large DC currents and vice versa. On the other hand, with a stationary puddle the heat input should be such that full penetration can be held long enough (about 5 minutes)to take data. The stationary experiments described here were performed on 2.5mm (0.1in) thick steel at about 60A DC (using a 3/32" diameter 30° tip angle tungsten electrode). On the same kind of plates, continuous welds are made with about 125A DC (at 3 in/min) and higher currents are common at higher torch velocities. The low level of the current has two important consequences: First, the resulting arc-force is much lower. Second, at low current the voltage-current relationship for the arc is quite non-linear, and this non-linearity affects the attempts to interpret the arc-voltage in order to detect the puddle motion.

On the other hand, a stationary weld is much larger in diameter than a continuous one. A typical diameter of a stationary puddle is 12mm, while a typical width of a continuous weld is 6mm. This difference coupled with the shape difference will affect the value of the natural frequency (probably higher for a continuous weld, since the puddle size, hence the mass, is smaller), and the magnitude of the motion under the same force (higher for stationary puddle, since the spring constant is slighly smaller for a larger puddle). Nevertheless, the stationary pool experiments represent an important first step in developing the ultimate control system.

4.2.4. Experiments

The purpose of these experiments was to perform a frequency response test on a fully penetrated weld puddle to identify the natural frequency of the puddle motion. The equipment used included a custom built solid-state current regulator with a 0 - 50 kHz bandwidth (for details see Section 5), a water cooled GTA torch, an FM tape recorder for recording ouput data, and an Hewlett - Packard 5423A Structural Dynamics Analyzer, which was used to compute the frequency spectrum information. In these experiments the arc pressure was used as the force input, and initially the puddle motion measurement technique was based on shadowing a laser beam by the back side of the depressed puddle.

In this measurement technique, a Ne/He laser beam is expanded through two lenses to a 1 cm diameter beam. After passing beneath the puddle the beam is concentrated (through a lens and a laser filter) into a photodiode (HP PIN Photodiode model 5082-4220). See Fig. 4.2 for a schematic of the measurement system. As full penetration is reached the puddle is depressed and blocks part of the laser beam. In response to a varying force the puddle moves up and down according to its dynamic characteristics, creating a shadow in the beam. The laser beam is then detected by the photodiode and its output varies according to the puddle motion.

Initially, the frequency of a 60A (peak to peak) sinusoidal component on a 62A DC current was varied in steps from 4Hz to 35Hz, and the photodiode

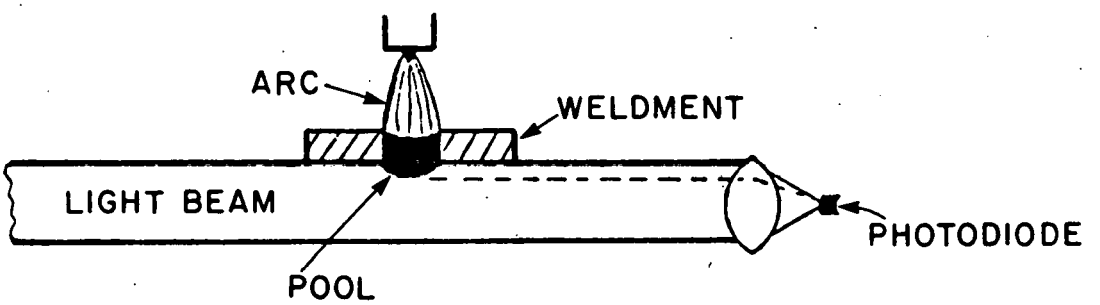

Figure 4.2 Schematic of the Laser Shadowing Puddle Motion Measurement Technique.

voltage was recorded on a chart-recorder. The resulting photodiode voltage (which was sinusoidal and of the same frequency as the input), increased in amplitude until about 14Hz, beyond which the output rapidly dropped off. (Phase angle was not measured.) This behaviour suggests the existence of a reasonance near 14Hz and indicates that the puddle acts like an underdamped dynamic system.

To permit a more exact determination of the puddle transfer function a broadband current control signal was constructed. In all cases the amplitude of the AC component in the current is kept at about 10% of the DC level (i.e. 12A peak-to-peak when the DC current is 60A). In this way linearity of the current-force relationship can be assumed.

During the experiments both the photodiode voltage output and the current measurement signal were passed through first order low pass filters at 200 Hz. before being recorded and the current signal (derived from the voltage drop across a resistor in series with the welding torch) was amplified by a factor of 100. The recorded data were then used as input to the HP Structural Dynamics Analyzer and the frequency domain information was obtained.

Typical results for the transfer function between the current input and the photodiode voltage output are shown in Fig. 4.3. Each transfer function was computed from data taken during the same experiment (same puddle), at different times after the initiation of the arc, and the plots are arranged in chronological order. The elapsed times after arc initiation for Fig. 4.3a, b, c, and d are 0,1.3, 2.3, and 3.4 minutes respectively. A peak at around 15-20Hz, and a -40db/decade roll-off are apparent in most of the graphs. The puddle grows slowly with time, and according to Eqn 4.1 the natural frequency is expected to become smaller. This phenomenon is demonstrated by the results since the magnitude peak clearly shifts to the left with time.

Fig. 4.4 represents results from a second puddle produced in a similar experiment. There is a clear peak in the amplitude at 18 Hz, and this peak is about 5.0 db. higher than the low frequency response. This corresponds to a damping ratio of about 0.3 and the natural frequency can be calculated from $w_r = w_n (1-\zeta^2)$. With w_r=18Hz this results in w_n=18.9Hz. Comparing with the numerical example given above for R=6mm there is a good agreement between this experimental value, 18.9Hz, and the predicted value (for R=6mm and $k=b_{oo}/R$) at 20.4 Hz. A -40db line is shown in Fig. 4.4 to be a good match to the roll-off after the 18Hz peak. This is in agreement with the expected second order system behavior.

From these results it can be concluded that the laser-based experimental technique is capable of detecting the puddle motion and that there is good agreement between the experimental results and the model of the puddle dynamics.

4.2.5. Discussion

With the existence of the puddle resonance confirmed it is possible to attack the problem of devising a practical means for detecting puddle motion. This was attempted here by using the same conditions as listed above, but in addition to recording the photodiode output, the arc potential was also

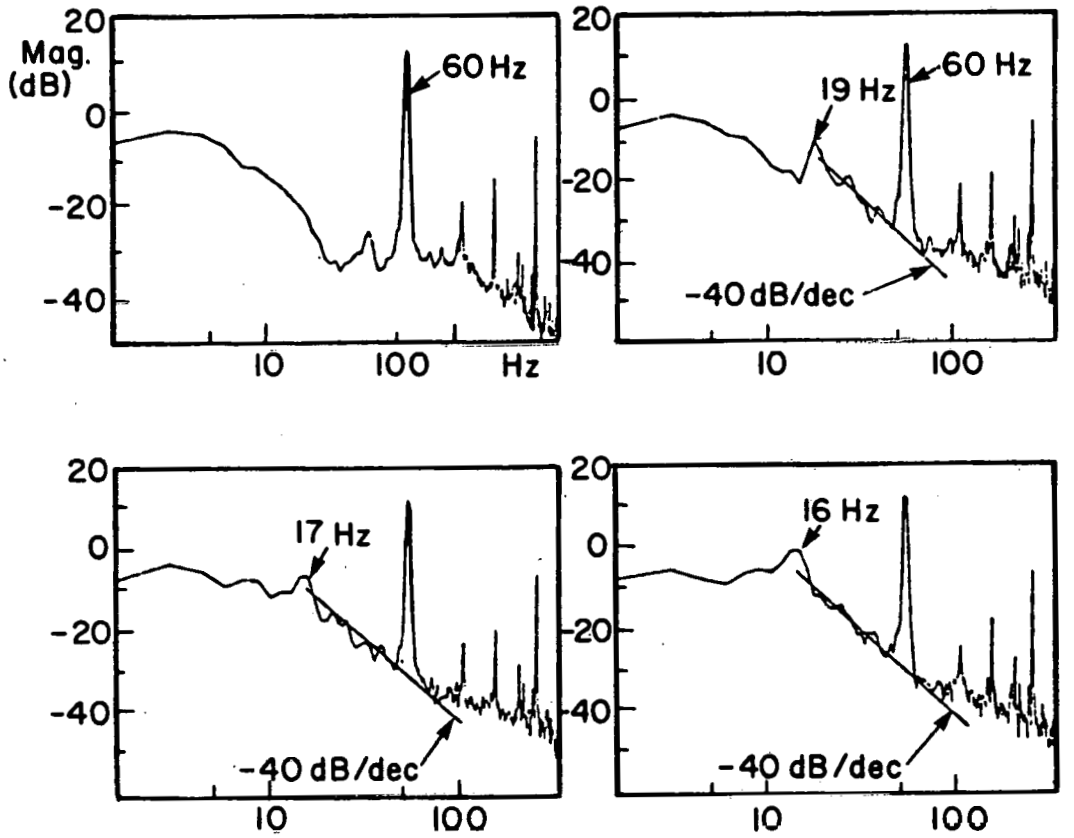

Figure 4.3 Transfer Function (Impedance), For a Single Puddle Evaluated at Different Times.

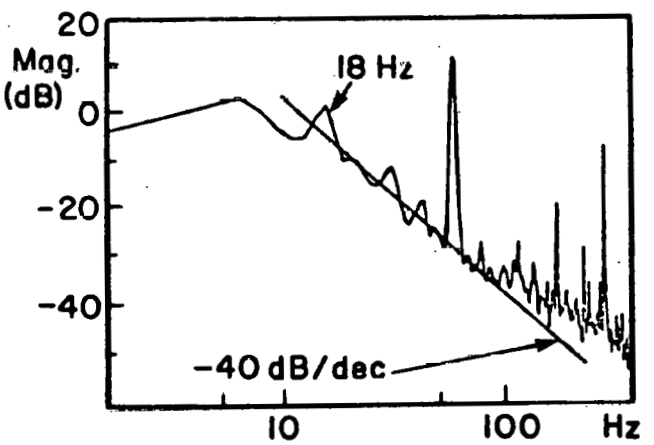

Figure 4.4 Puddle Impedance, Second Puddle

recorded. To improve the arc-length change related signal to noise ratio the voltage change resulting from the current change (assuming a linear V-I curve) was subtracted from the measured arc voltage.

With this procedure it was possible to get frequency spectra from the arc voltage that suggested the second order characteristic detected earlier, however, these results were not consistent. The major problem was the fact that the DC arc current had to be maintained at a low level because of the stationary puddle geometry and this necessarily keeps the arc force low. Furthermore, the arc voltage-current relationship at low DC currents is highly non-linear, which makes interpretation of the voltage measurement more difficult. It is expected that with the higher current typical of moving torch welding that the resulting arc-length related voltage variations will give more consistent frequency response data. (For more details on the arc-voltage measurement problem see Zacksenhouse [4.7].)

4.2.6. Implications for Control System Design

The weld puddle size measurement method developed here is intended for use in a real-time feedback regulator. Accordingly, the feasibility of such an application must be addressed. Since the proposed measurement technique involves identifying low frequency resonances, the time required for such a measurement will be long relative to the desired response time of the system. This presents the classical problem of large measurement delays in the feedback path.

To investigate the effect on a weld puddle frequency (size) regulator, a discrete controller was designed based upon a first order model for the weldment melting dynamics and using a proportional plus integral (PI) control strategy. The frequency measurement was modelled as a delay of n time steps of the controller where n is governed by the required resolution of the frequency measurement. For a frequency resolution of 1 Hz, a plant time constant of 1 sec. (as reported by Garlow [4.5]) and a sample time of 0.1 sec., the PI controller was designed using Z-plane root locus techniques.

The feedback measurement delay caused most designs to be marginally stable, but one in which the controller zero cancelled the plant pole gave acceptable performance. The disturbance response of this design for a value of the controller gain that gave the smallest settling time is shown in Fig. 4.5. This illustrates a 5% settling time of 30T or 3 seconds. For a puddle length of approximately 6mm this settling time suggests a maximum velocity change of 6mm/3sec or about 6 in/min, which is a reasonable velocity for thick section GTAW. Therefore, for a first order performance evaluation we can conclude that the torch will not overrun the weld pool during the disturbance settling time.

It must be noted that the pole cancellation design will have some severe limitations when applied to the real system, since the plant pole is a highly variable parameter. Consequently this problem is an ideal candidate for parameter adaptive control.

4.2.7. Conclusions

A technique for measuring the size of a fully penetrated weld puddle has been presented. It requires that the frequency of oscillation of the

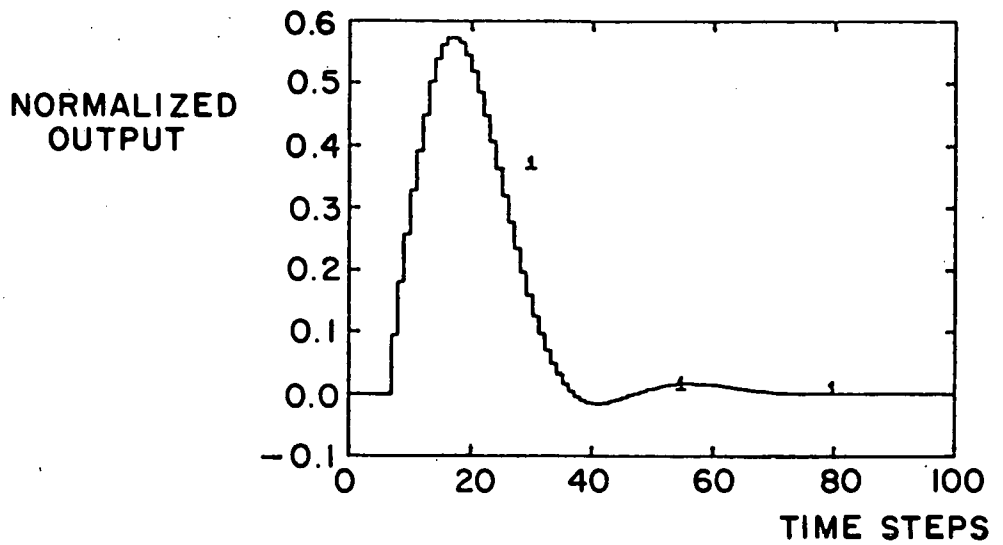

Figure 4.5 Step Disturbance Response of the System Using Pole-Zero Cancellation (The Output is Normalized to the Plant Gain "A").

puddle-surface tension system be identified in real-time and then regulated using the torch velocity as the control input. The basic ability to excite and detect the puddle natural frequency has been demonstrated, however, this has only been done for the case of a stationary weld puddle. It remains to be seen if similar results occur when a moving torch is used. Also, the essential relationship between natural frequency and puddle size has yet to be examined experimentally.

Preliminary controller designs based on real-time FFT identification of the puddle natural frequency indicate that satisfactory response can be obtained despite the long time delays involved in the sampling-transformation process, but the use of adaptive control schemes may be necessary.

4.3. A Simple Penetration Control System

As a more immediate control signal we have been investigating the use of the steady state puddle depression that results when full penetration occurs. By measuring this steady state puddle depression when welding horizontally, we have been able to effect a rudimentary closed loop controller for maintaining a full penetration weld. The puddle depression upon complete melting is measured by looking for an increase in arc voltage (under conditions of constant current and constant electrotrode workpiece separation). This voltage increase is a result of an overall arc column length increase caused by the puddle depression. In simple experiments with stationary puddle created by a TIG torch, as the puddle goes from partial to full penetration, the arc voltage can be seen to increase rapidly by nearly 0.5 volts.

A penetration control system was devised to exploit this signal, and is illustrated schematically in Fig. 4.6. This "bang-bang" controller will regulate to an average full penetration weld by continuously decreasing or increasing the local heat flux according to whether or not full penetration is detected. As shown in the figure, the feedback sensed is the arc voltage, and when a certain threshold is exceeded, full penetration is assumed. In response to full penetration, the heat input is reduced until the voltage goes below the threshold. At that time the heat input is again increased. By always seeking the full penetration transition, the adaptive qualities of the controller are realized since any change in the welding conditions, such as thickness or heat conductivity, will be reflected in a change in the point of full penetration. This change will be tracked by the controller thereby maintaining full penetration despite the disturbance. With this admittedly simple control scheme, the weld depth will be forced to oscillate about full penetration, but the amplitude of the oscillation may be minimized by proper selection of controller parameters.

A preliminary experiment with this control scheme has been performed and the results follow closely the predicted performance of Fig. 4.6. In this experiment the torch voltage was sensed by a microcomputer, filtered to remove unwanted electrical noise, and then compared to a threshold voltage (which was determined automatically, right after torch start-up). The result of the comparison (i.e. above or below threshold) caused the computer to command a torch velocity increase or decrease (which was effectively a heat input decrease or increase).

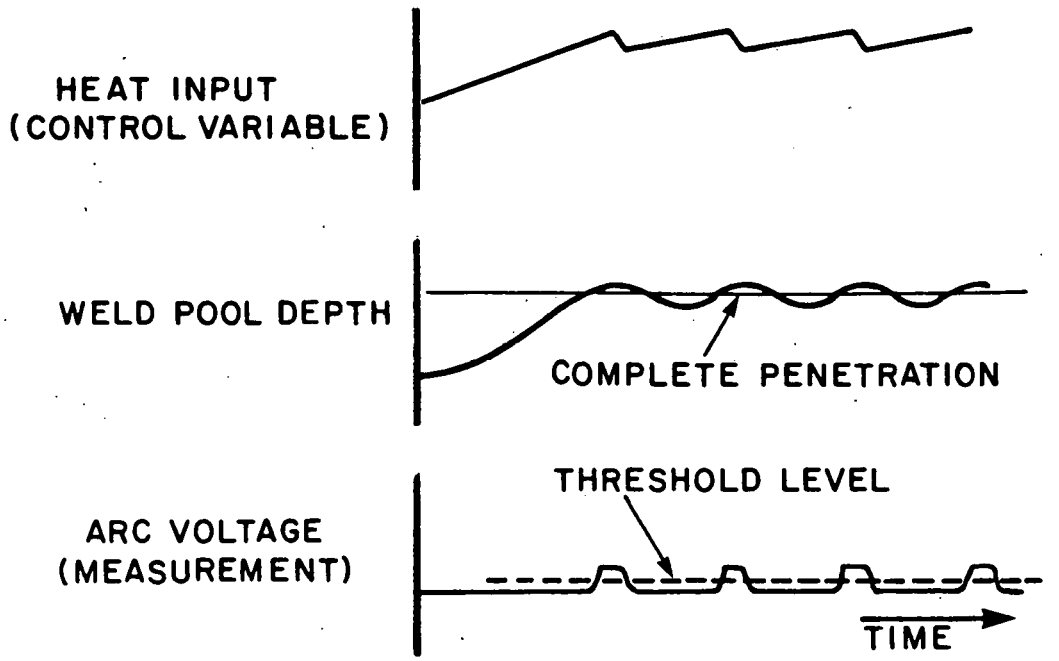

Figure 4.6 An On-Off Penetration Control Scheme.

A typical result is shown in Fig. 4.7, where the expected changes in arc voltage are seen driving the torch velocity in an oscillatory fashion. The resulting weldment showed periodic full to partial penetration as expected. The oscillation is more severe than desired, because after full penetration has been obtained, the effective heat input must be significantly decreased before full penetration is lost. Nevertheless, some degree of control of penetration has been achieved without the need for any specific sensors.

In summary, we are exploring two methods of full penetration sensing, and have demonstrated the use of the steady state puddle depression measurement in a closed-loop penetration control experiment. The results verify the utility of this measurement for control but also point to the need for further refinement in both the measurement technique (e.g. to provide anticipatory information about full penetration) and in the control algorithms to be used with this measurement. We expect these refinements develop from both basic studies of arc physics and arc-puddle interaction.

4.4. Real Time control of Backbead Width

In an effort to examine the dynamics and control problem associated with closed-loop control of full penetration welds, we have conducted an investigation based upon direct backside measurement of backbead width. In doing so the dynamics of weld pool melting and controller performance have been considered, and actual computer controlled welding tests have been performed.

4.4.1. The Sensor

As mentioned earlier, a useful technique for measuring the width of the back bead is direct optical sensing. This can involve a visible imaging system, a thermal imaging system or a simple light intensity measurement. We have initially pursued the latter since it provides adequate measurements for control experiments, and is the simplest method.

The actual measurement is the intensity of visible light emitted by the back bead, and the device used is shown in Fig. 4.8. The key features are the narrow "slot" transverse the weld that confines the view of the sensor to a thin transverse section of the back bead. In this way the light received comes from a well defined portion of the back bead, and as the width of the bead increases, the amount of light passing through the slot should increase, regardless of changes in other dimensions of the bead. However, the intensity of radiation received will depend not only on the viewing area, but also on the temperature of the bead. In order to provide a simple output from the phototransistor that is receiving the radiation, it is desirable to eliminate the temperature effects. Although this cannot be completely accomplished. it can be shown (see Garlow [4.5]) that by eliminating the infrared portion of the radiation by the use of optical filters, combined with the limited spectral response of the phototransistor, greatly minimizes the temperature effects. As a result the lower temperature areas that are in view (the unmelted weldment) do not significantly contribute to the output. However, reliable operation still requires that the temperature distribution of the weld pool be constant, which is quite often not true. As a result, this sensor requires frequent calibration, and does inject errors depending upon the size of the weld, the torch travel speed, and the preheat of the

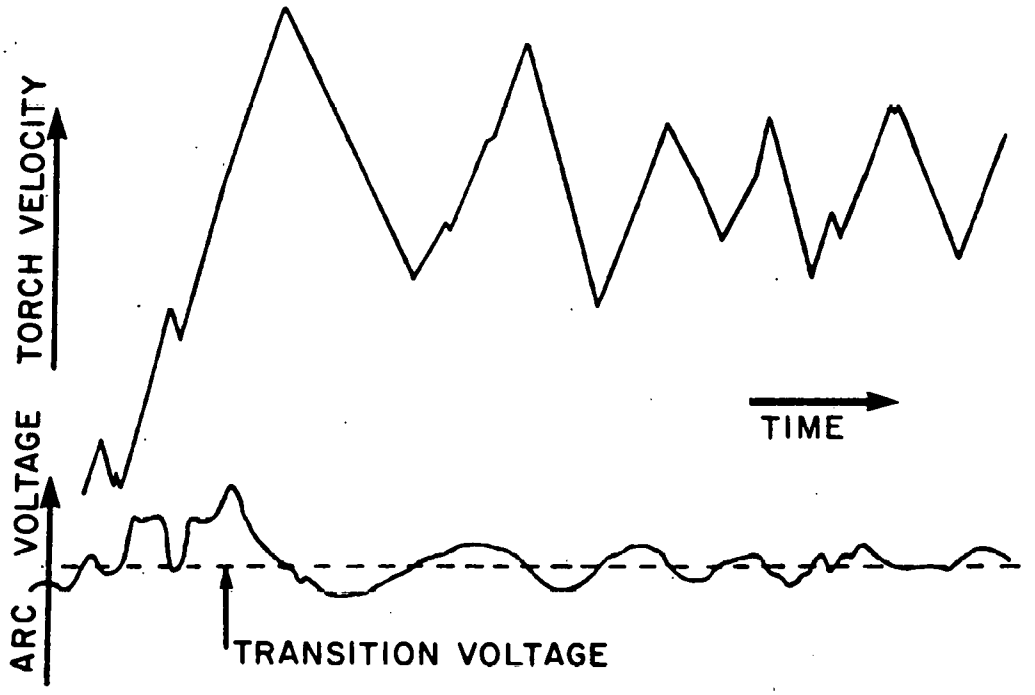

Figure 4.7 Experimental Results Using the Scheme Shown in Figure 4.6

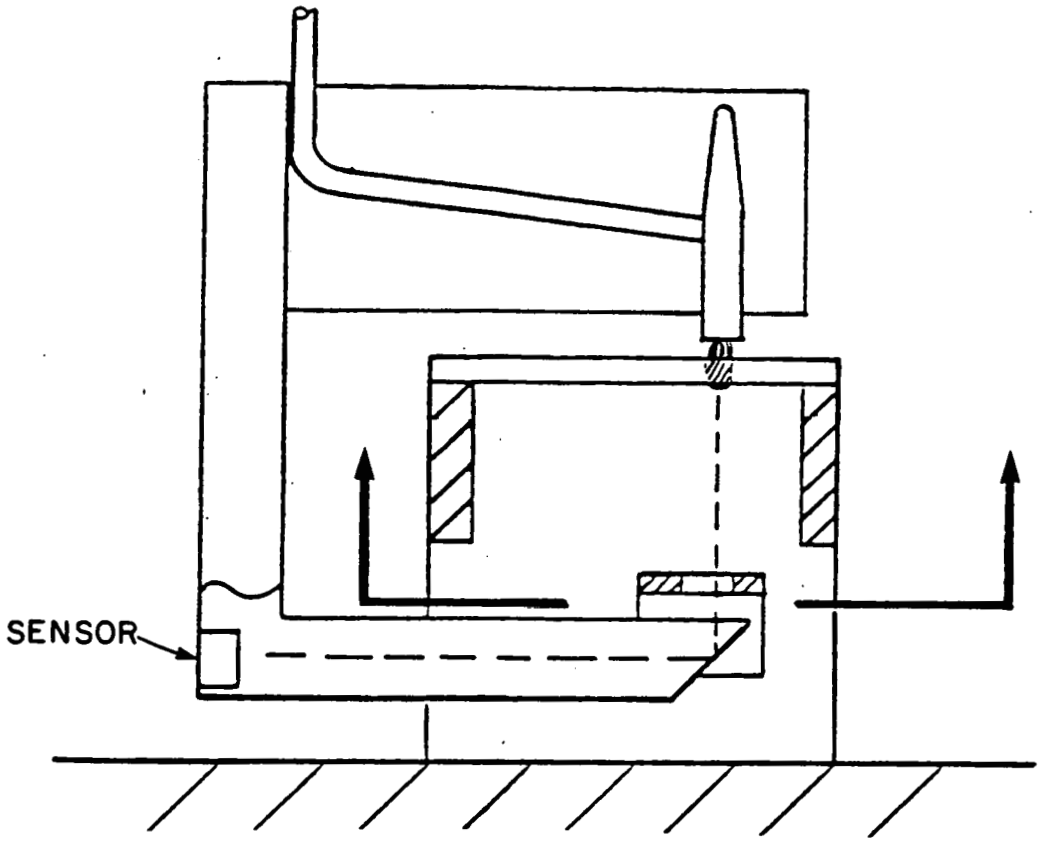

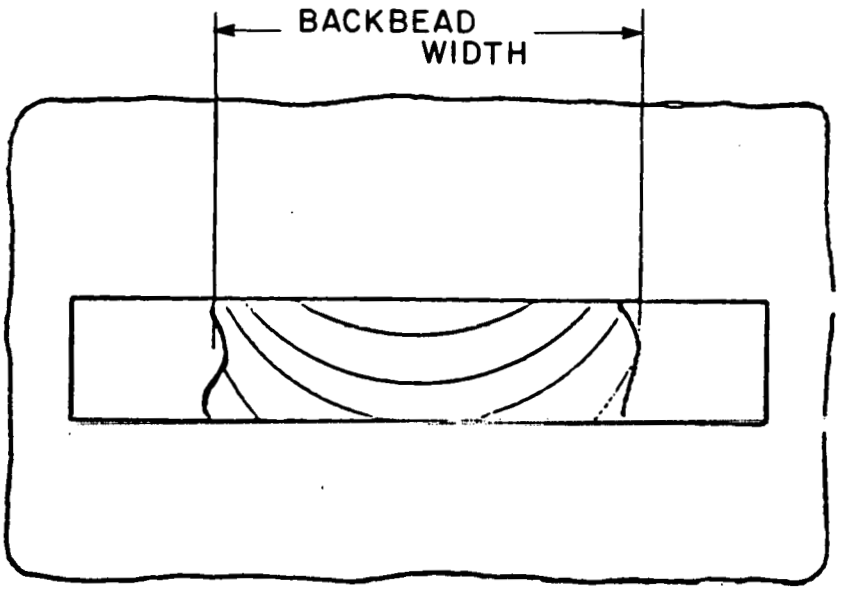

Figure 4.8 The Optical Back Bead Width Sensor

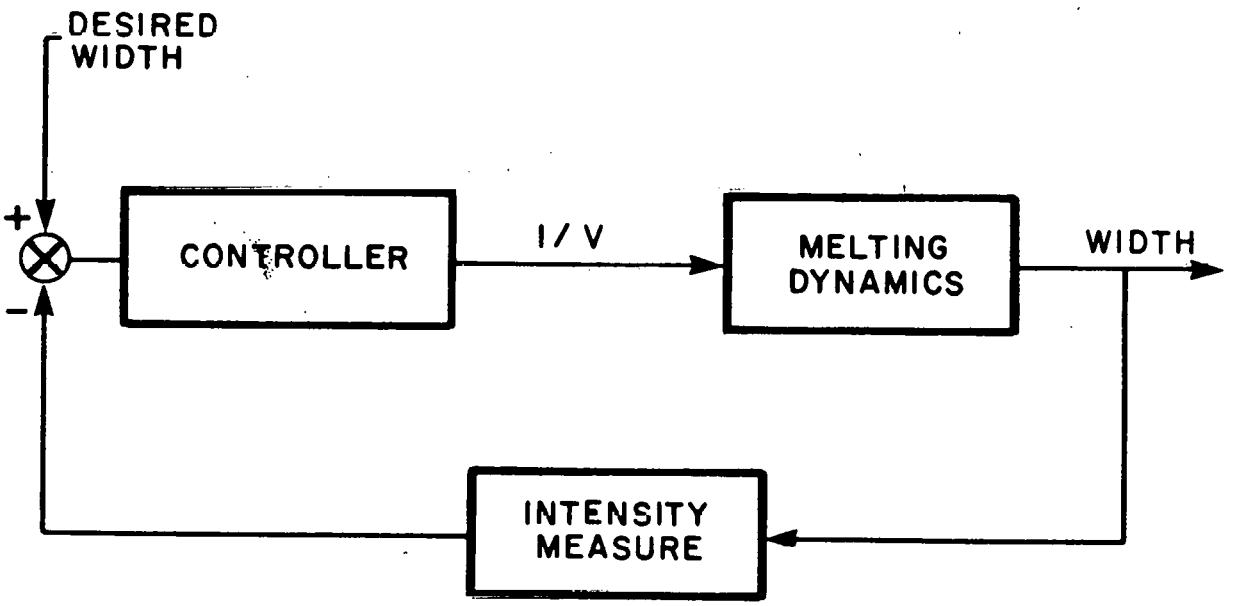

Figure 4.9 Block Diagram for a Back Bead Width Regulator

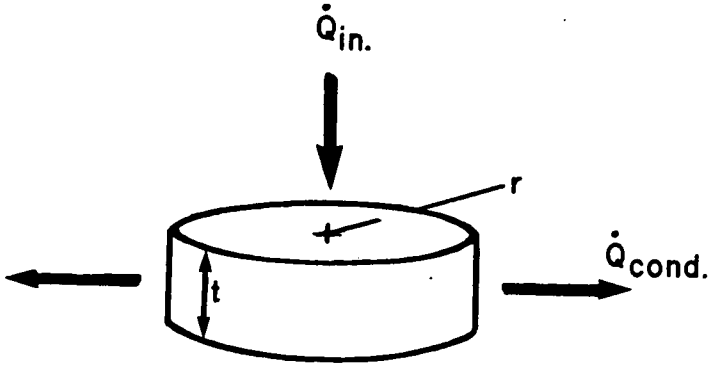

Figure 4.10 Weld Pool Heat Transfer Model

weldment. In addition, the presence of impurities on the surface of the molten back bead creates a random fluctuation in the light output. This is reflected in a noise level on the phototransistor output that at present limits the performance of the control system. Despite these drawbacks, however, the simplicity of the sensor and its output make it highly useful for control studies, which will be described below.

4.4.2. The Control System

Given a simple analog sensor for back bead width, a width regulating control system can be designed. Such a control system is shown in Fig. 4.9. However, before the control system can be designed, a model of the dynamics of the process must be defined. To this end a simple model of melting dynamics was developed to relate the torch heat input to the resulting back bead width.

In a series of tests where torch speed was changed in a stepwise fashion, the back bead width was always observed to monotonically approach its new value, and a first order linear response was suggested. With that form in mind the following model was constructed.

Consider the pool geometry and resulting heat balance shown in Fig. 4.10. Assuming that all heat lost from the pool is by conduction to the solid weldment, the heat balance takes the form

$$Q_{in} = Q_{cond} + \rho c_p \frac{dV}{dt} \qquad (4.2)$$

where Q_{in} is the net heat input to the pool, Q_{cond} is the heat conducted through the weldment, and ρ, c_p and dV/dt are the density, specific heat and rate of change of volume of the pool repectively. This indicates, as expected, that if Q_{in} and Q_{cond} are equal the pool will be stationary in size, and otherwise will change in volume according to the difference between the heat rates. Thus for a given heat input Q_{in}. changes in the conducted heat will determine the dynamics of the weld pool dimension.

For the idealized cylindrical geometry of Fig. 4.10, the heat conducted from the pool can be roughly approximated by considering the temperature gradient across the solid liquid interface, and the conduction area available. Thus we can devise the pool radius dependent conduction term:

$$Q_{cond} = k\ 2\pi\ t\ r\ dT/dr \qquad (4.3)$$

Where k is the thermal conductivity of the weldment, the second term is the radius dependent heat transfer area and dT/dr represents a local temperature gradient.

If we now express the pool volume in terms of the thickness (t) and the cylindrical pool radius (r), and substitute Eqn 4.3, we get the desired relationship between heat input and pool width (or radius):

$$(\rho c_p 2\pi\ t\ r)\ dr/dt + (k\ 2\pi\ t\ dT/dr)\ r = Q_{in}$$

or

$$C(r,t)\ dr/dt + G(k,t,\ dT/dr)\ r = Q_{in} \qquad (4.4)$$

where C(.) is a non-linear capacitance and G(.) is a non-linear conductance. Q_{in} is the net torch power = $\eta E\ I$; η=torch efficiency, E is the arc potential and I is the welding current.

Thus the model indicates a non-linear first order relationship between heat input and pool radius. If we assume for the moment that C and G are constant, and take the Laplace transform of Eqn 4.4, we can get a transfer function relating the input to the output:

$$\frac{\text{Radius}}{Q_{in}} = \frac{K}{\tau s + 1} \qquad (4.5)$$

where K= 1 / G and is a gain term; and τ = C / G, and is the system time constant.

Notice that the torch speed does not explicitly appear in this equation. the major impact of velocity is on the "net" temperature gradient driving the conduction away from the pool. According to this model the width is affected by the torch speed not by virtue of the term Qin , but by a change in the conductivity parameter. This indicates that control using torch speed will be inherently non-linear as opposed to using the current. If we make an approximation that the conductivity (G) is directly proportional to the torch speed (v), then the response of the width (r) to speed changes can be interpreted. Since the conductivity term is the zero order parameter in the basic differential equation, changes in K will have two effects: 1) the steady state value of the width will change even for a fixed value of Qin, and 2) the time constant of the response = C/G will change. Therefore with the torch voltage and current fixed, changes in v will cause an apparently linear response from the system, except that the time constant of the response will depend upon the magnitude of the change in k.

To develop a linear transfer function for control purposes where torch speed rather than current is the control input, it can be shown [4.8] that the same first order form given above is appropriate provided the input quantity is 1/v rather than v. Given this basic control model it is necessary to experimentally identify values for the gain (K) and the time constant (τ).

The experimental procedure for determining K was to create a full penetration weld using a TIG torch travelling at constant speed, and then measure the resulting steady-state back bead width. As expected this gain was not constant, but showed a strong dependence upon the anount of preheat, which directly affects the gradient $d\tau/dr$. From Eqn 4.5 we expect to have a higher value for K as the preheat increases, and this was observed in the experiments. Also, as the thickness (t) decreases, we also expect the gain K to increase, which was again born out by experiment. Finally, when using 1/v as the control input quantity, changes in current now appear directly as changes in the system gain.

Determining the time constant involved changing the torch speed in a stepwise fashion and evaluating the resulting width response. This can be done by looking at the initial slope of the response, determining the time to reach 63% of steady-state, or by fitting an exponential response curve to the data. The latter proved the most reliable, and was chosen for these tests. The results indicate that the time constant is indeed a function of the pool radius and of the preheat, however, the strength of that effect is not as strong as the model may have implied. (Details of these experiments are contained in Weinert [4.8].)

4.4.3. Control System Design

In order to design a linear regulator for this system, a constant parameter model must be assumed. From a control system design perspective the above model assigns first order dynamics to the process, however, the parameters of this model, K and τ are non-constant, thus a constant paramter control system can be expected to yield variable performance. Parameter adaptive control can be applied to remove this variation, and a preliminary study of this nature has been conducted by Reiff [4.9], however, only constant parameter control system results will be discussed here.

Given a nominal value of τ = 1 second for 11 gauge carbon steel welded at 100 amps, and 15 volts, a regulator design study was performed. It was decided that a proportional- integral controller design was most suitable since, for a first order process, it provides zero steady state error and allows the roots of the system to be arbitrarily specified. Using nominal values of K as determined by experiment, a PI control system was designed and implemented on a computer controlled welding system. This system is shown in Fig. 4.11 and allows the computer to input the width sensor voltage, operate on this with the control program, and output the appropriate table velocity command. The table speed is then controlled by a DC servo system of high accuracy and bandwidth.

The controller was evaluted in two ways: frequency response and step response. In the former, a sinusoidally varying command width was input to the controller, and the response of the width recorded. The results are shown in Fig. 4.12, and they indicate that the system responds as expected, i.e. a second order characteristic, indicated by the -40 dB/dec slope beyond the natural frequency of the system. This confirms the basic assumption that the melting dynamics can be described by a first order model.

The next set of tests involved issuing a step change in the desired width of the regulator and examining the resulting response. From Fig. 4.12 we expect that the response will involve an overshoot with quick settling to the desired final value. The results of such a test are shown in Fig. 4.13a, where it can be seen that the expected transient was indeed observed. However, as the amount of preheat increased, and the command value of width was changed, the nature of the response, also changed as is shown in Fig. 4.13b. to a preheat 100°C. Note the change in overshoot and settling time of this response. This indicates that the process model parameters(specifically the gain and time constant) are indeed varying as predicted by the model and open-loop tests.

This study indicates that when a control loop is closed about the bead width, non-linear dynamics are encountered which will tend to make control

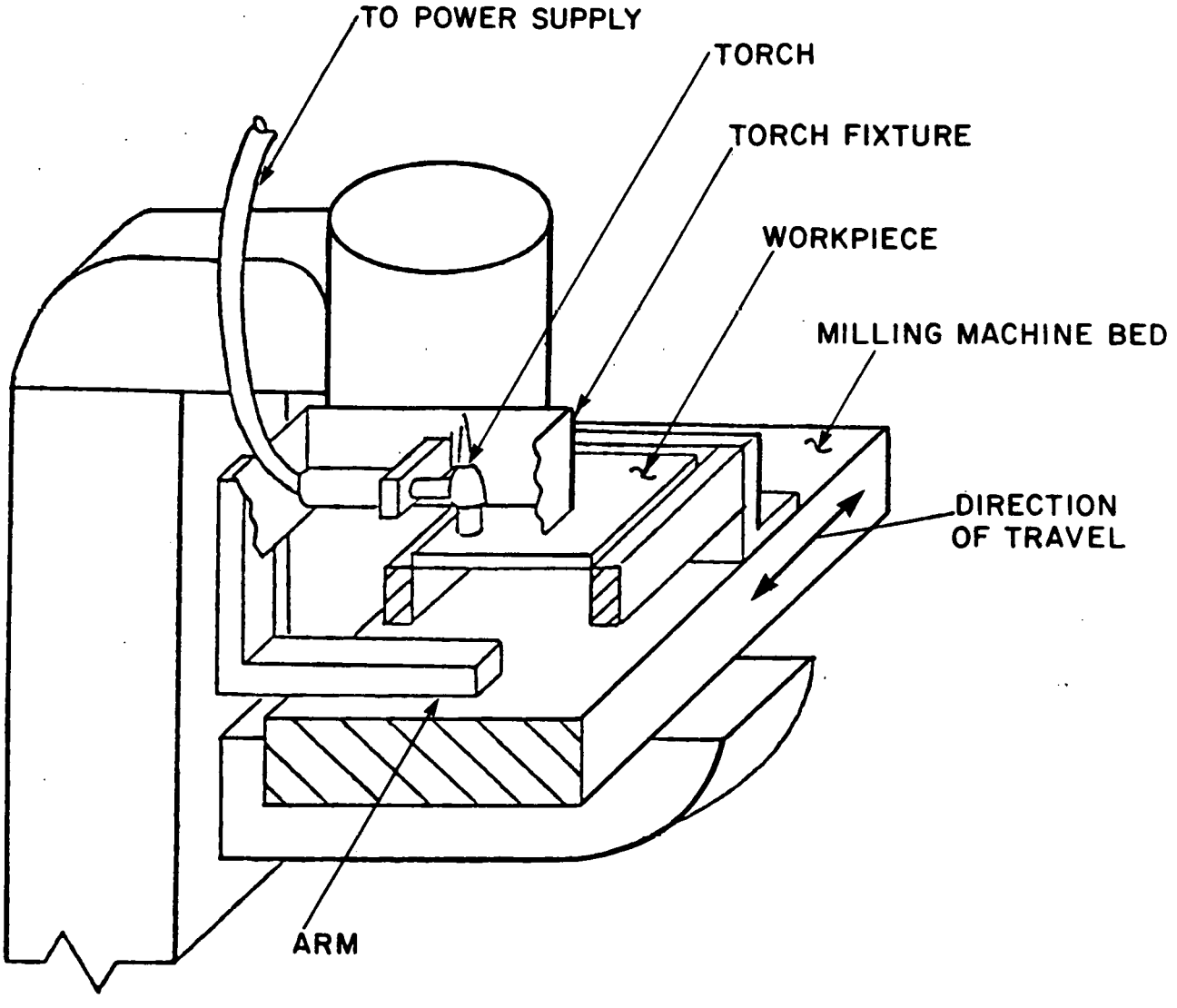

Figure 4.11 Welding Control System.

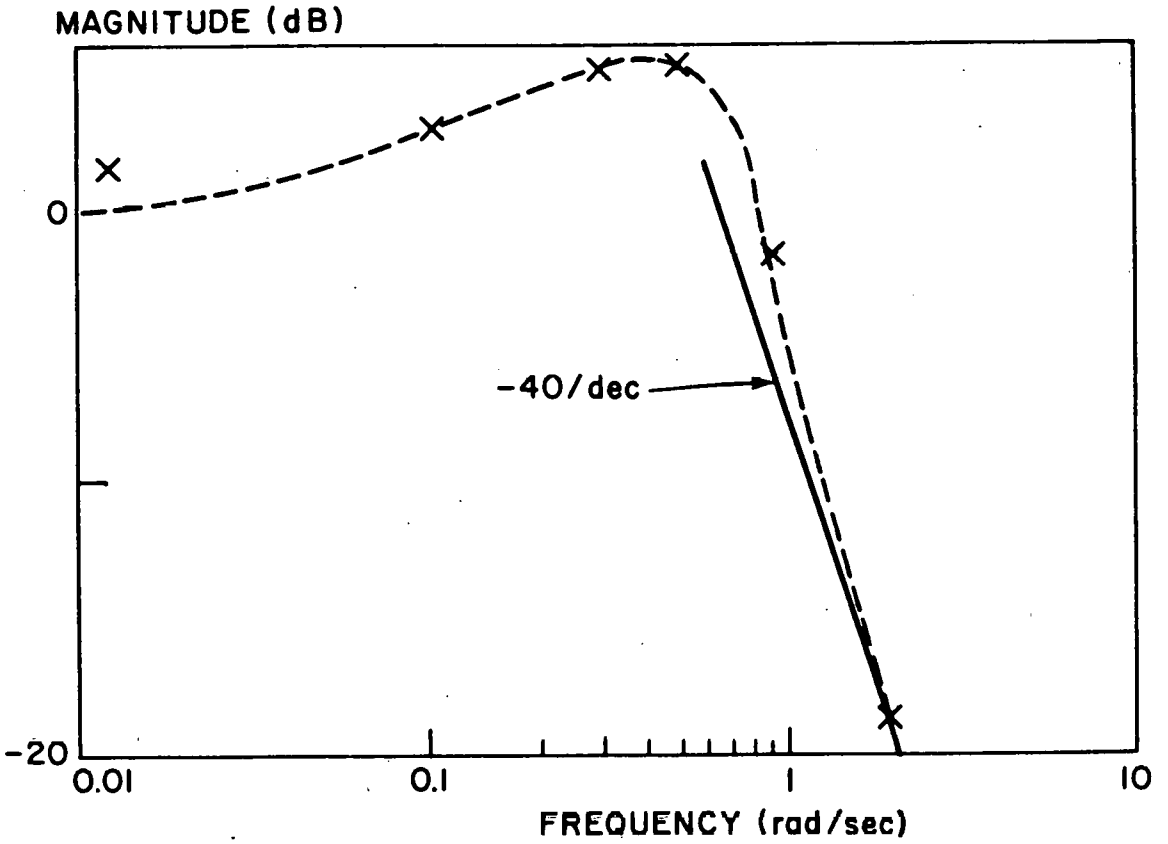

Figure 4.12 Closed-Loop Frequency Response of the Back Bead Regulator Using PI Control.

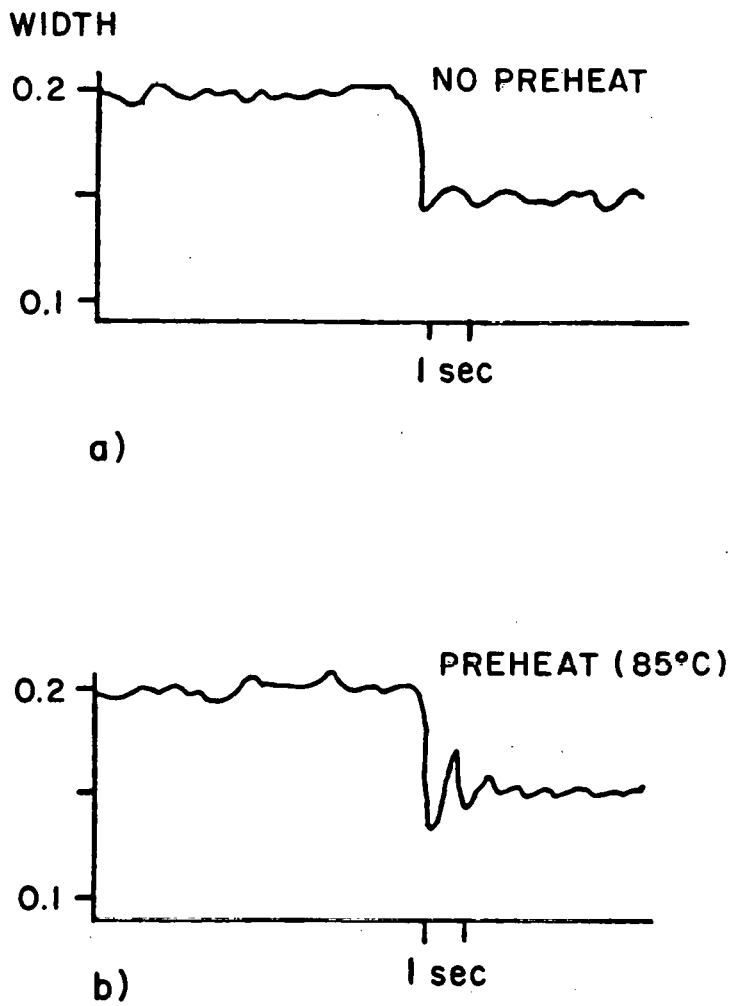

Figure 4.13 Step Response Using PI Control;
a) No Preheat b) With Preheat.

system response inconsistent. This has been demonstrated by experiments. However, despite this uncertainty, good steady state width regulation can be achieved. The only penalty is that speed of response to unknown disturbances will have to be compromised to insure smooth response over a wide operating range of the processes.

The results of this controller design are also directly applicable to any control system for back bead width. As practical topside sensing methods are developed, such as that described in Section 4.1, final control system design can proceed directly based upon the control model and confirming experiments described here.

5. Weld Puddle Geometry

Within the context of control of weld geometry it is important to understand and develop computationally simple models to predict the puddle size. The weld puddle geometry is affected by a variety of parameters including the geometry, the thermal input and the fluid motion interior to the puddle. The general situation is shown schematically in Fig. 5.1. The importance of the geometry and the heat input is easy to understand, although it is not necessarily trivial to determine the actual puddle size from first principles. Stirring type fluid motion in the puddle can be caused by several possible phenomena including a) density gradients caused by temperature gradients, b) shear and normal forces exerted on the puddle surface by the plasma flow, c) surface tension forces resulting from the nonuniform surface temperature, and d) electromagnetic stirring forces caused by expansion of the current from the electrode spot size to the area available for current conduction out of the solid. Elaborate numerical calculations have been performed for some conditions related to GTAW, but while these are important in understanding the phenomena, they are inappropriate for control purposes. The results of measurements and analysis indicate the complexity of the problem and indicate that different phenomena dominate under different conditions. In our work we initiated predictive or correlative models for puddle shape. For these studies a stationary puddle configuration was chosen, and experimental and analytical work was performed. The analytical model was used to deduce the nature of fluid motion in the puddle which was required to result in the measured shape. The results underscored the complexity of the puddle motion and provided some insight into development of the control level models.

5.1 Experimental Measurements

The basic set-up used a stationary welding torch in conjunction with a stationary work piece of a circular slab of steel cooled by a water-cooled copper ring, as shown schematically in Fig. 5.2. The torch characteristics (voltage and current) and the heat transferred to the water coolant were measured. The puddle top width was measured from the projected image of the puddle surface on a screen and the puddle depth measured indirectly by monitoring the rear-face temperature with a Pt-Pt 13% Rh thermocouple. In addition, for a limited set of torch conditions the test piece was removed, cut, polished and etched with a 5% Nytol solution to show the fusion line.

Plates of 1/5" and 3/8" thickness were machined into disks to yield aspect ratios (radius to thickness) of 1 to 1, 2 to 1 and 3 to 1. For the initial experiments a standard welding power supply (Aircromatic Welding Machine Model CV-450) was used and the current was set to a constant value for each data point. Experiments with controlled current pulsing can be done, but have not been completed at this time. A 1/8" diameter 2% thoriated tungsten electrode was used and was shielded by a 22 cfh flow of argon (purity 99.99%) passed through a 2304-0074 nozzle.

The variation of rear face, centerline temperature is presented in Fig. 5.3 and shows the temperature increasing roughly linearly with power dissipated in the arc. With the exception of the smallest diameter plate, the rear face temperature was higher for a thin plate with a particular aspect

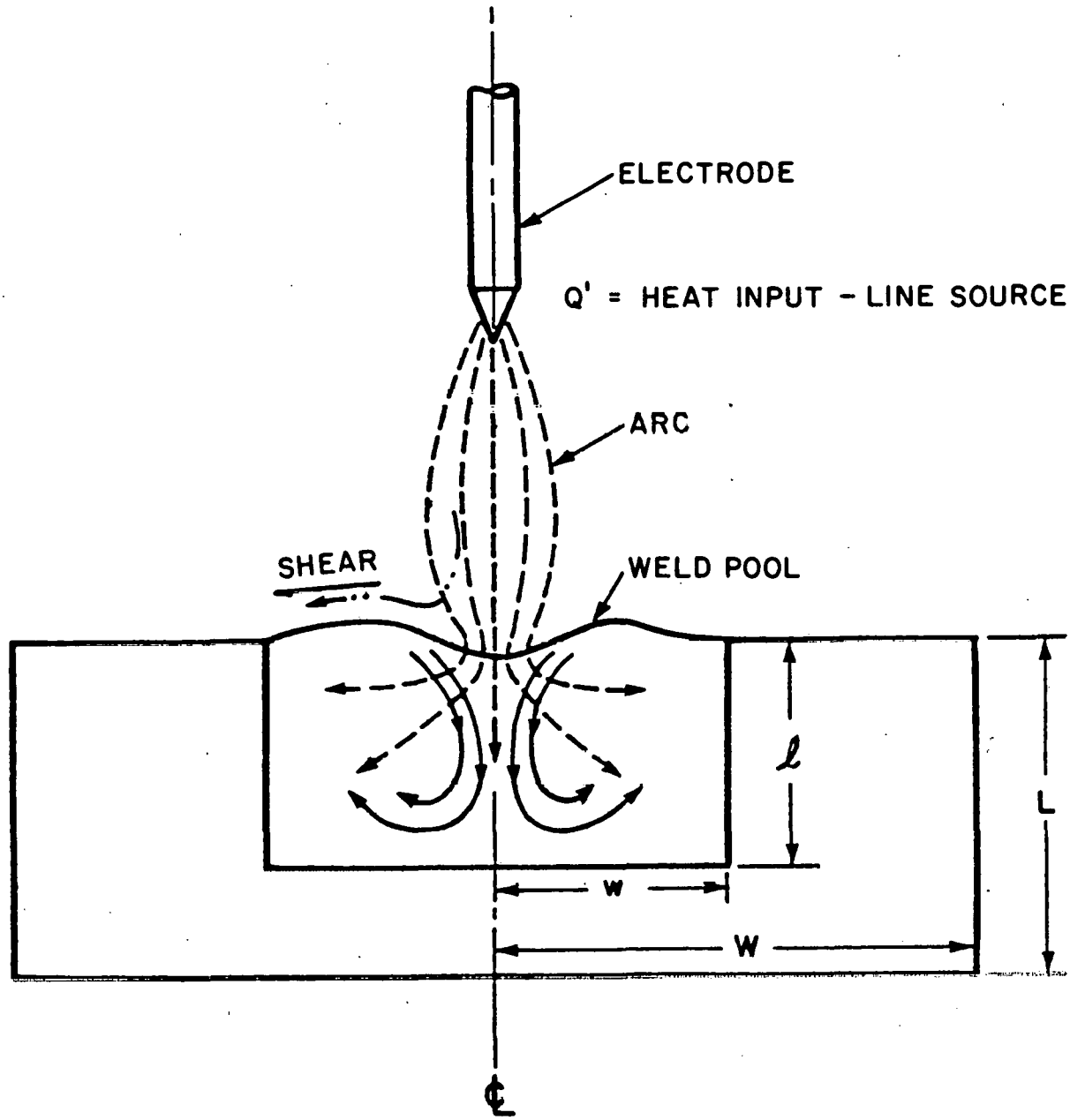

Figure 5.1 Schematic View of Weld Puddle.

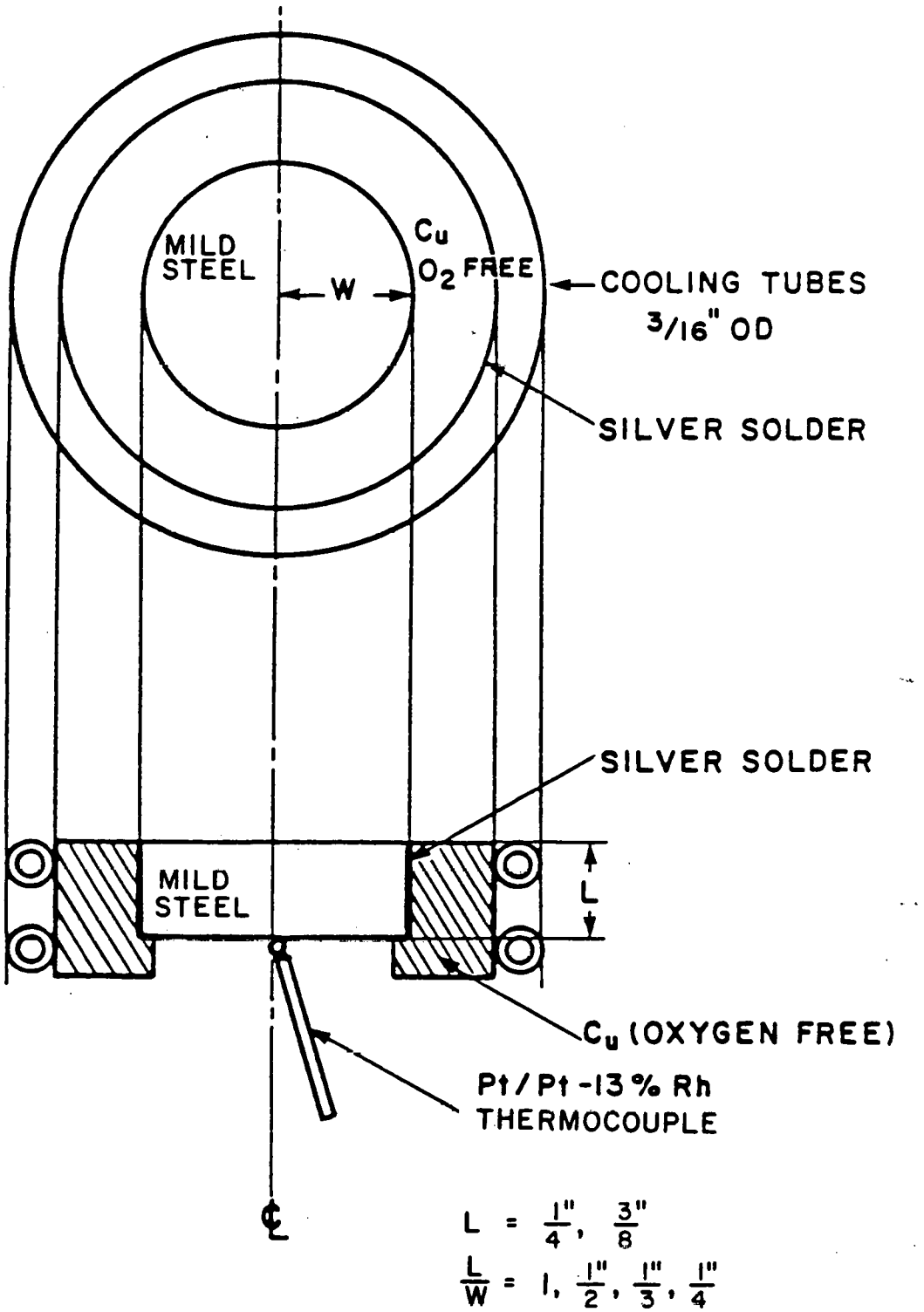

Figure 5.2 Sketch of Work Piece Holder and Cooling Piece.

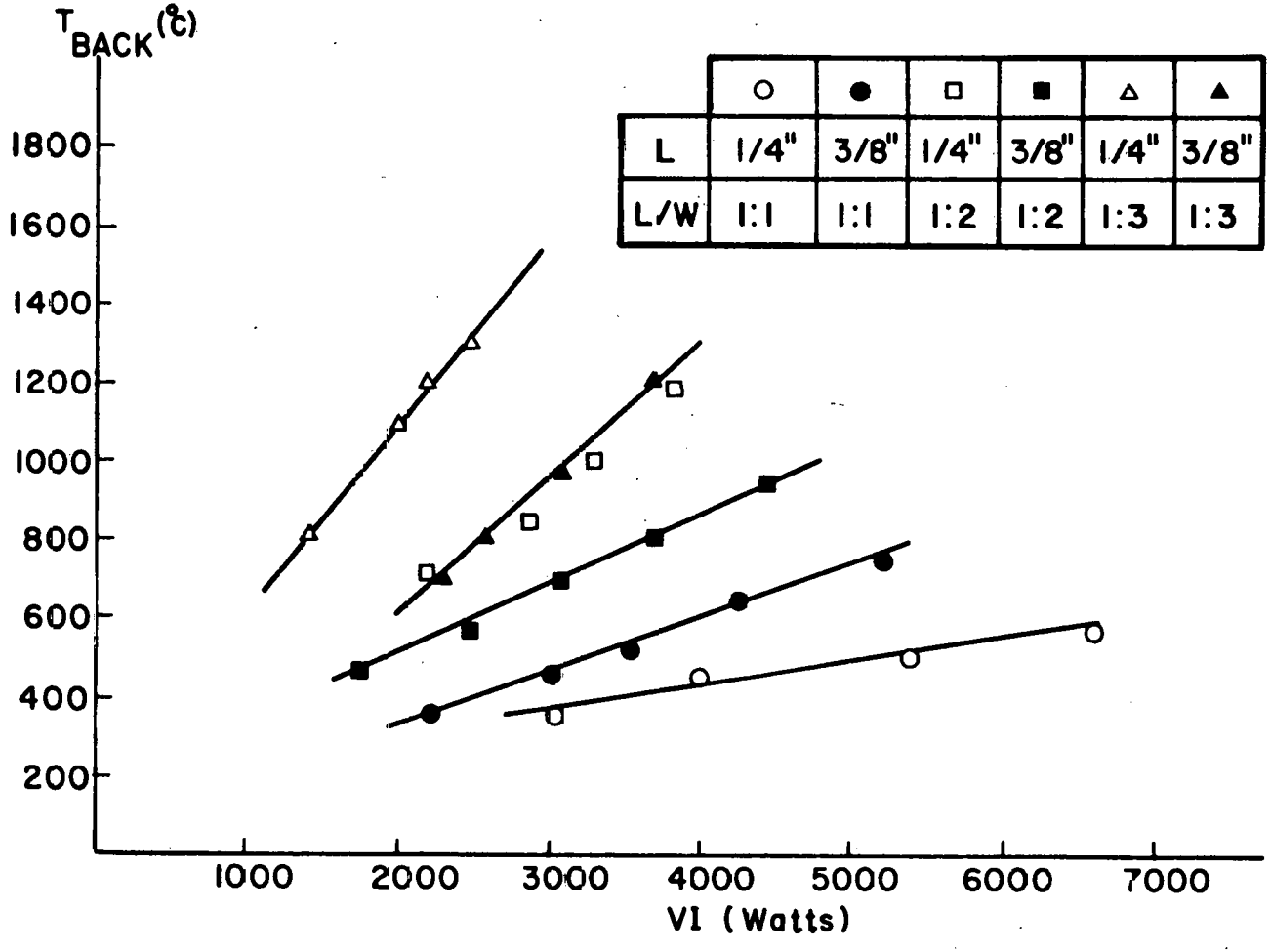

Figure 5.3 Back Temperature as a Function of the Weld Torch Power (VI).

ratio, than for a thick plate at the same aspect ratio. If the arc efficiency were constant, this would indicate that a change in the extent of stirring accompanies the change in size. The variation of puddle diameter at the torch surface with arc power is shown in Fig. 5.4. For the larger diameter plates there is little difference between the puddle width at a particular power. The anomalous results obtained at the 1 to 1 aspect ratio may have been caused by the "lip" (see Fig. 5.2) supporting the steel disk, which in the case of the 1/4" diameter case was a substantial fraction of the disk diameter.

The puddle shape was measured by the etching technique for 3/8" thick disks with aspect ratios of 1:1, 1:2, 1:3 and 1:4. The results are presented in Table 5.1 and indicate that the ratio of puddle depth to puddle half diameter increases with disk aspect ratio. In all cases the weld pool was larger in radius than it was deep.

While not extensive, these results represent data that can be used to deduce some of the characteristics of the interior flow.

5.2 Analytical Modeling

Many interpretations and analytical models are based on a strict heat conduction situation as represented traditionally by the Rosenthal theory. Measurements and analyses have clearly shown that fluid motion is an important factor in determining the pool shape. Rather than determining the fluid flow from first principles; in this preliminary work we developed a model which, for an assumed circulation in the weld pool and heat input, would calculate the weld pool geometry. In practice, we used this model in the inverse; that is we used the measured heat input and weld pool shape to determine the sense and strength of the weld pool puddle motion.

The solution is divided into two sections: conduction in the solid material and conduction/convection in the weld puddle. The conduction solution is effected by conventional finite difference techniques and the weld puddle solution by a simplified heat exchanger type solution. The two solutions are coupled and solved iteratively for the weld pool motion. At present a two-dimensional cartesian solution is used to approximate the two-dimensional cylindrical symmetric situation.

Conduction Solution. Symmetry allows reduction to the half width geometry shown in Fig. 5.5. The outer face in contact with the cooled copper ring is assumed to be at the coolant temperature of 290 K. The lower surface is assumed to radiate as a grey body with a specified emissivity. To determine the sensitivity to radiative losses, cases have been run with an emissivity ranging from 0 to 1. The weld pool is approximated as a rectangular shape and the temperature taken as the melting point of steel i.e., ~ 1620 K. The difference equations were written and the resulting matrix inverted to find the node temperatures. The total heat rate into the bottom face (labeled B in Fig. 5.5) and the side (labeled A in Fig. 5.5) were then computed from the node temperatures. These heat fluxes were then used to determine the fluid flow in the weld pool.

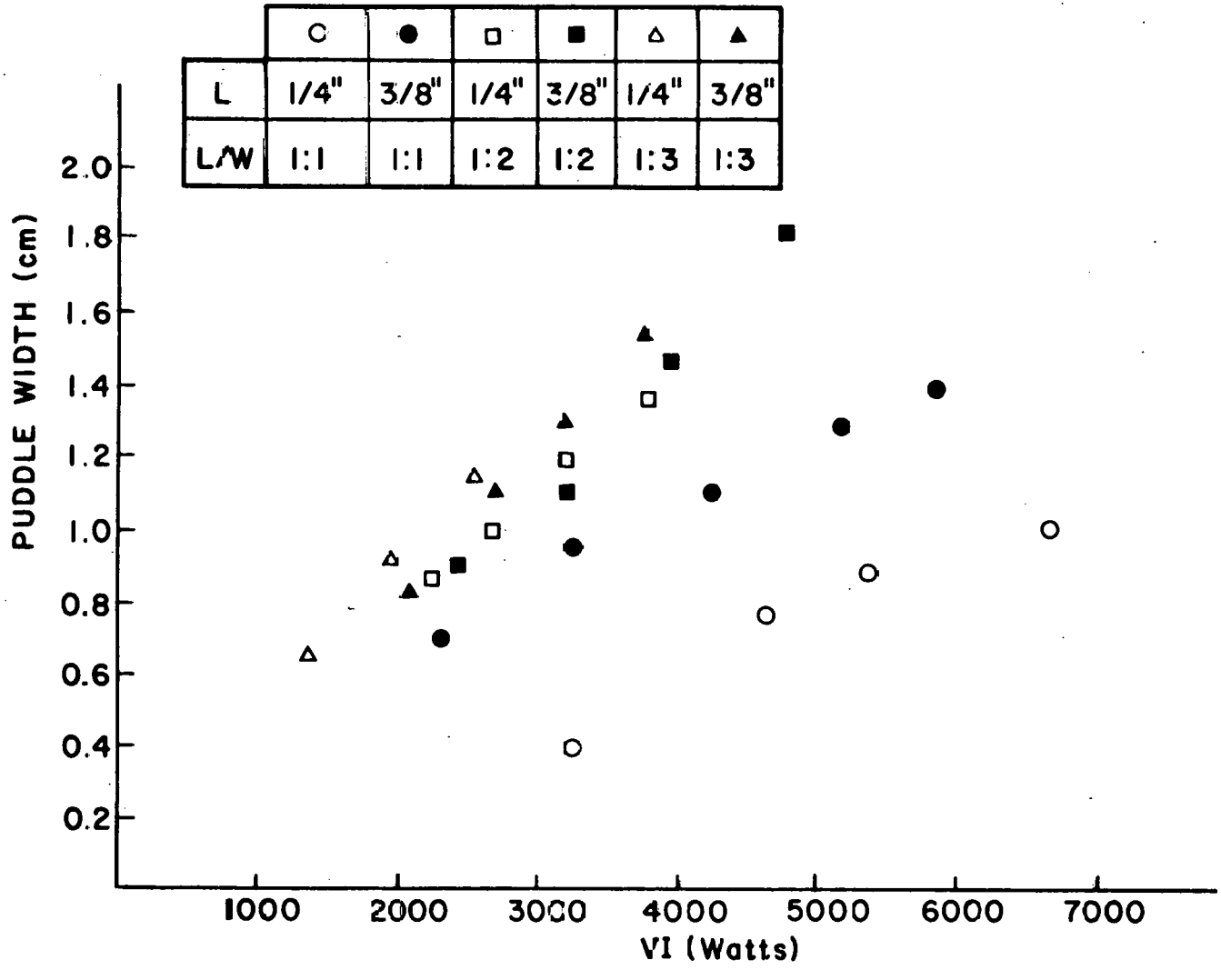

Figure 5.4 Puddle Width as a Function of Weld Torch Power (VI).

Table 5.1 - Results of Puddle Shape Measurements

	Ratio of Workpiece Thickness to Radius			
	1:1	1:2	1:3	1:4
Puddle Depth mm	4.82	5.38	6.86	7.62
Half Puddle Width mm	7.49	7.72	8.38	9.08
Aspect Ratio Depth/Half Width	0.64	0.69	0.82	0.84
Arc Power kw	2.3	2.1	2.0	——

Weld Pool Model. The weld pool is considered as a heat exchanger type flow where the pool material is heated in the region near the arc spot and then cooled as it passes the pool boundary. The situation for the case where the fluid flow is downward from the arc spot is shown in Fig. 5.5; this is the expected situation if the self-induced electro-magnetic forces in the weld pool dominate over gravity, surface tension and plasma jet surface forces. By specifying the criculation rate of the fluid the heat transfer coefficients for the flow to the surfaces can be computed. Then, if the maximum fluid temperature is assumed to be equal to the boiling temperature of the material, the heat rate to the side and bottom walls can be computed. The circulation rate is varied until these values agree with the values required by the conduction solution. Details of the technique are described in Reference 5.1.

The influence of circulation on the pool shape is shown in Fig. 5.6 where the pool depth and half width are plotted as a function of the average fluid velocity. In this case the fluid flow is down from the arc spot toward the bottom surface. As expected, the stagnation type flow against the bottom surface increases the heat transfer toward the bottom and results in deeper weld pools. The model also indicates that significant variation in puddle aspect ratios are achieved at average speeds of the order of 1 cm/sec..

Recommendations. The results obtained are quite preliminary and not extensive. Nonetheless, the indications are that the basic approach is reasonable. We expect to continue these experimental efforts, concentrating on the effects of current pulsing on pool shape.

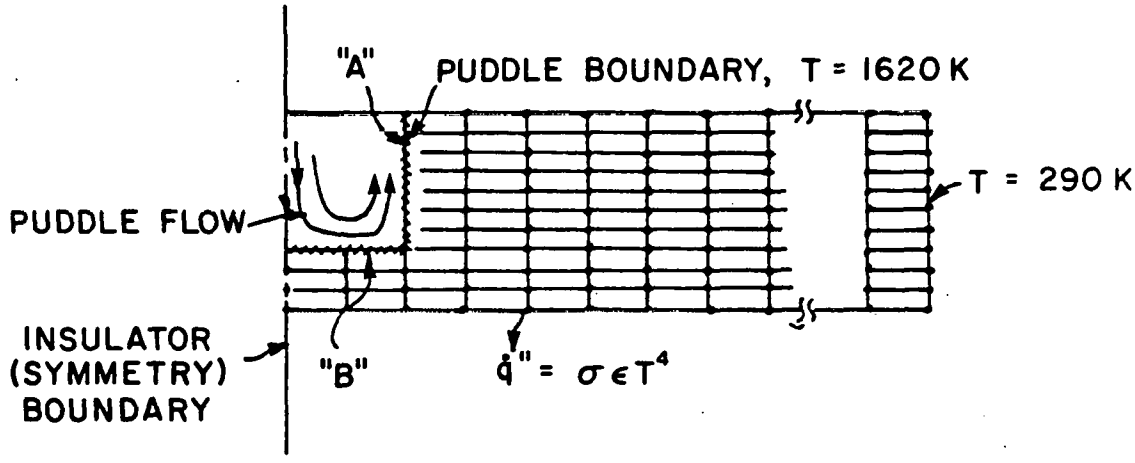

Figure 5.5 Sketch of Geometry and Boundary Conditions Used for Numerical Solution.

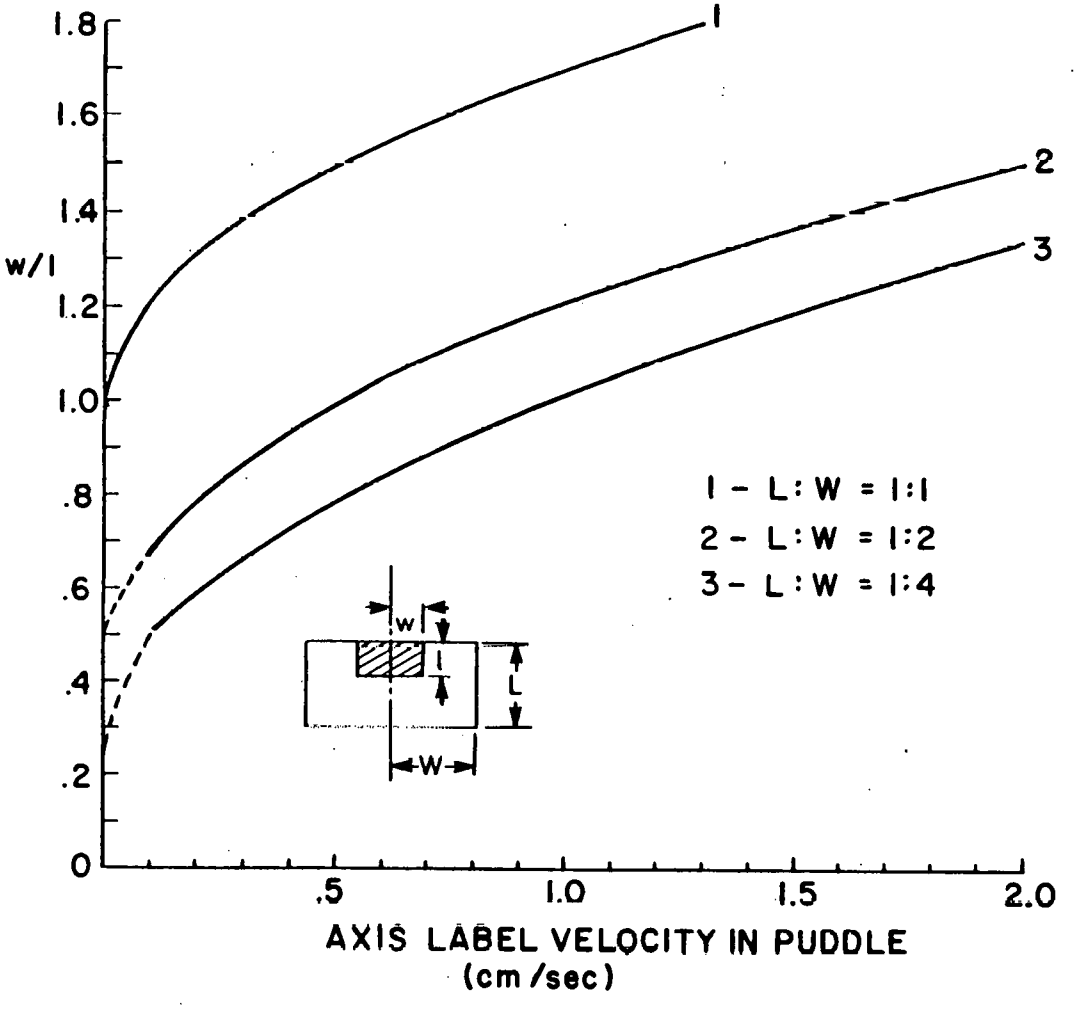

Figure 5.6 Weld Puddle Aspect as a Function of Velocity for Different Base Material Aspect Ratios.

6. Arc Current Regulator

Control of the static and dynamic current level to the welding arc is a necessary part of a closed-loop controlled welding system. In addition, accurate control is especially necessary when detailed scientific experiments such as those described in the previous sections are performed. After examination of the available power source controller concepts, a power transistor regulator was chosen to control the output of a conventional three-phase rectified welding supply. This approach is to be contrasted with other solid state power supply regulators based on SCR's. Specifications were written for the device and a sub-contract awarded to Alexander Kusko, Inc. After installation in the laboratory, modifications were made (in consultation with the personnel from Kusko) to achieve a faster time response. This section describes briefly the design and operation of the controller. Further details are presented in Reference 6.1.

6.1 Basics of Operation

The basic function of the current regulator is to control the current through the arc. This is accomplished by connecting a transistor bank in series with the arc and with the power supply and then controlling the voltage drop across the transistor bank. A simplified schematic is shown in Fig. 6.1. Another way to consider the circuit is to view the transistor as a current amplifier. The current to the base of the transistor(s) is amplified and forms the main current to the arc. In this way the problem of controlling the main welding current is reduced to controlling the much lower magnitude base current. A feedback current controller is used to control the base current to the reference value. The actual current through the arc, as measured by a current shunt in the current controller, is compared with the reference signal, and the base current adjusted accordingly. The reference signal is provided either by a ten turn potentiometer or from a remote analog input. The remote input is suitable either for a function generator or for the A/D output of a computer.

6.2 Choice of Transistor and Control Circuit Configuration

The power output stage of the current regulator used 96 model 2N6258 transistors in parallel. A schematic of the transistor power supply is shown in Fig. 6.2. Multiple transistors were used rather than a single transistor rated at the full power because it was felt that this approach would achieve the best frequency response. Also, the smaller transistors were advantageous in that their delivery time was shorter, the potential for costly damage was less, and it was easier to reject the power dissipated in the smaller transistors. A second current amplifier stage was also constructed using the model 2N6258 transistors and is labeled T2 in the figure. A final stage (T3) connects to the output of the control circuit. The transistor bank is rated at 60 V maximum and 300 A continuous current.

One input to the controller circuit is from the current shunt which has an output of 100 mV at the full current of 300 A; the second input is the reference signal for which 10 V is to correspond to the full current of 300 A. A block diagram is shown in Fig. 6.3. These signals are scaled to 0 to 1 volts full scale signals by precision multiply-by-ten and divide-by-ten circuits respectively. The two 0 to 1 V signals are subtracted to form an

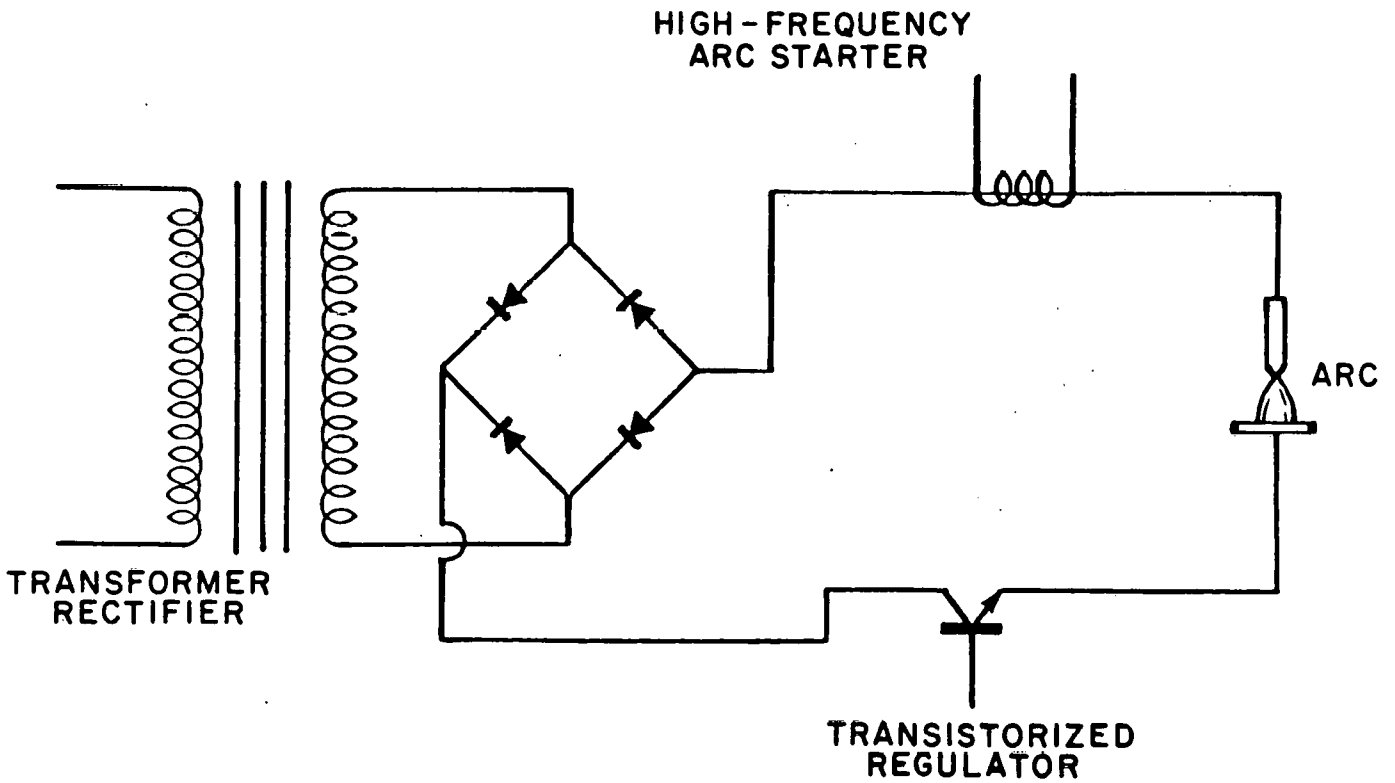

Figure 6.1 Power Source Configuration.

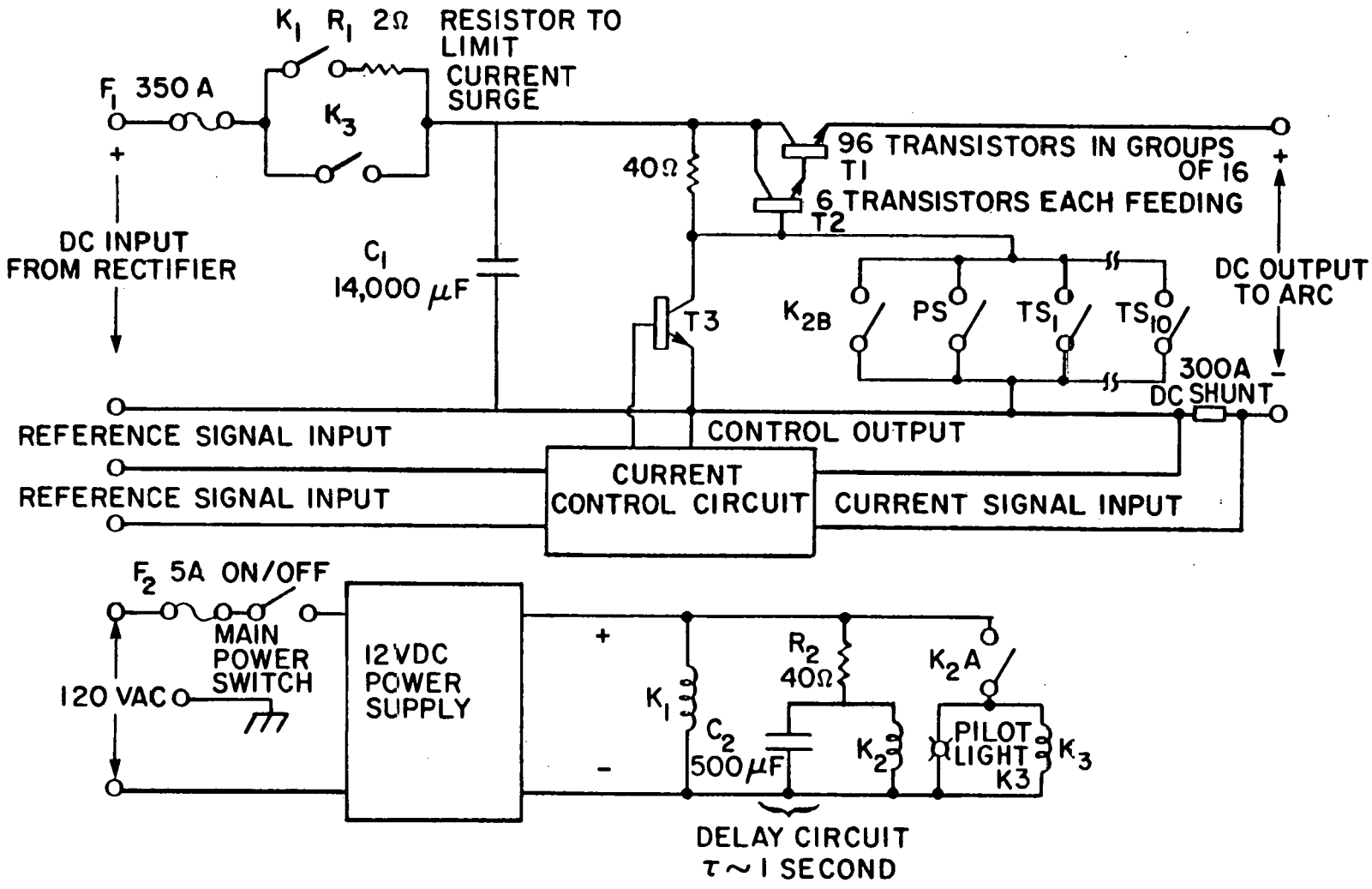

Figure 6.2 Schematic of the Current Regulator Showing the Protection and Sequencing Circuit.

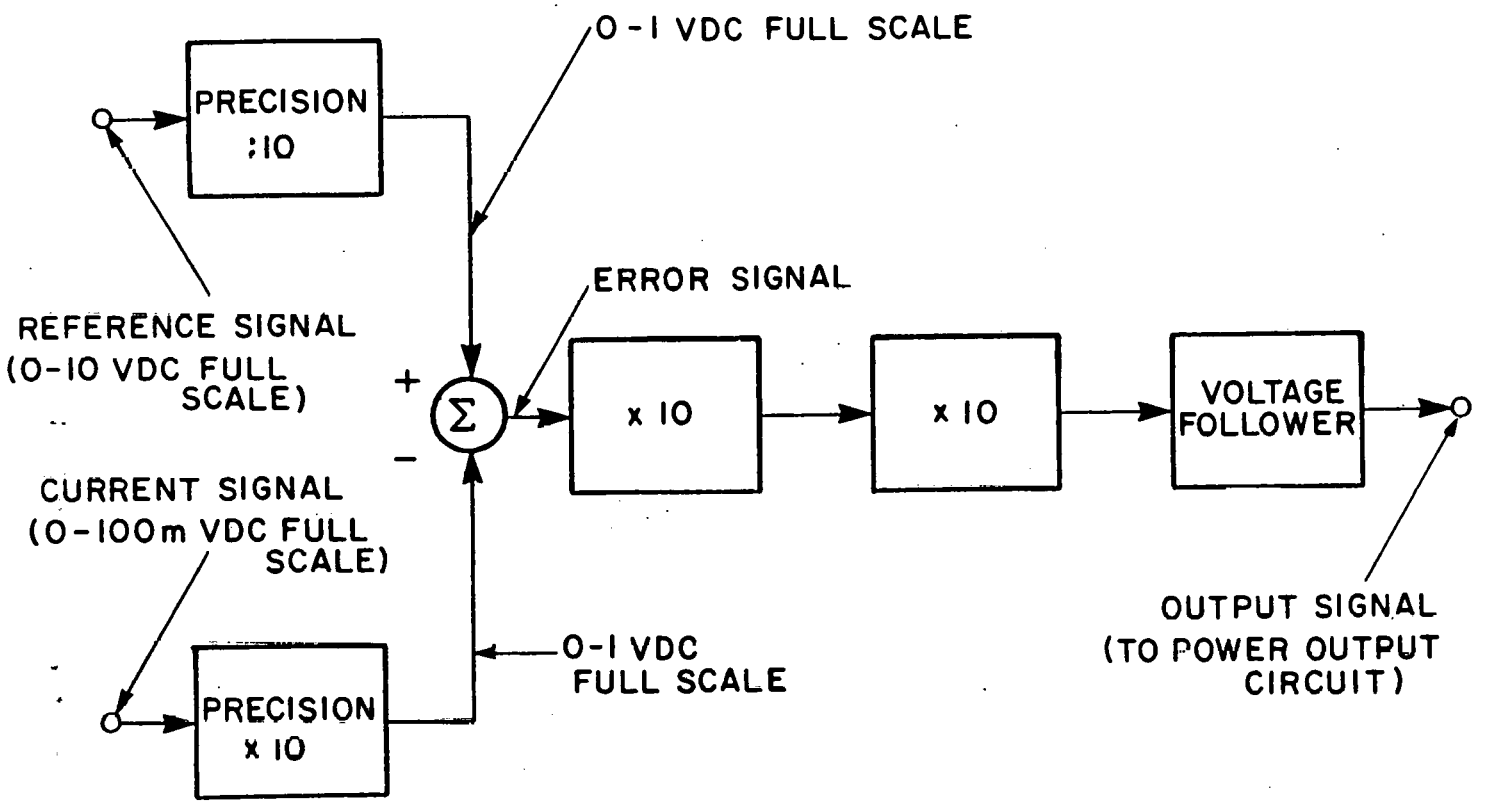

Figure 6.3 Block Diagram of the Current Control Circuit.

error signal which is multiplied by 100 in two successive multiply-by-ten amplifier circuits. This signal is then amplified by a voltage following circuit and finally by the base current sent to the first stage of transistor amplifiers (T3).

As delivered, the regulator used a standard model LM 741 OPAMP for all stages of amplifiers of the control circuit. Since the gain-bandwidth product of the LM 741 is 1 MHz, each of the latter gain stages was limited to a gain of 10. This results in a regulator maximum bandwidth of about 100 kHz, such that a feedback bandwidth of 20 kHz could be achieved. The experiments studying plasma jet transients required faster response, so the controller was modified. The OPAMPS in the last two voltage gain stages were replaced by model 318 OPAMPS which have a higher gain-bandwidth product and a higher slew rate. These amplifiers are more prone to instabilities than the LM 741 OPAMPS and a frequency compensation circuit was used to adjust the step response of the regulator. In addition, an offset adjustment was provided to establish the zero level. With the faster amplifiers, rise times of 15 sec were obtained for a step variation in arc current of 60 A. This was satisfactory for the arc studies.

6.3 Regulator Protection Circuitry

Water cooled heat sinks were provided to cool the transistors in the main bank and the additional gain stage. Each device is expected to operate at a maximum power dissipation of 100 W yielding a total dissipation of 9600 W. Each heatsink has a thermal switch which is part of the protection circuitry. A water flow of about 5 GPM was normally provided to the regulator.

A protection circuit automatically disables the power output circuit i.e. reduces the output voltage to 0 V, when one of the two conditions occur:

1) loss of water pressure in the cooling system; or

2) the temperature of any of the heat sinks rises to a dangerous level.

The protection is achieved by shorting the output from transistor T3 through the appropriate switches. Switch PS is closed if the water supply pressure is too low, and switches T_1 through T_{10} are closed if the temperature of the particular heat sink rises above a dangerous level.

The protection circuit also holds the power output circuit disabled for a period of 1 second following the turning on of the rectified power supply input. This delay period is used to charge a capacitor bank in the current regulator to the potential of the dc input bus voltage, thus avoiding the high current surge which would result from placing the uncharged capacitor bank directly onto the input bus. The protection is achieved by operation of relays K1, K2 and K3. When the power supply is turned on switch K_1 is immediately closed, thus allowing the input capacitor to charge through the delay circuit R_2-C_2 charges. Until relay K2 is activated switch K2B is closed, the output from transistor T3 shorted and the current regulator is disabled. When relay K2 is closed (after about 1 second) switch K_2B is opened and switch K3 shorts out the 2 resistor; the regulator is fully activated. This delay period also allows the 15 V power supply used by the regulator

circuit to stabilize, such that the regulator is operational when the power output circuit is enabled. The low power supply in the regulator floats with the negative terminal of the welder; since the positive (workpiece) terminal is usually provided, the power supply circuit changes potential when the main rectified power supply is activated.

A radio-frequency arc starting protection circuit was also provided with the regulator. Although it was later found that the standard protection circuit provided as part of the arc starter was more than adequate to protect the transistor current regulator, the custom protection circuit was useful in that it by-passed the coil of the arc starter and thereby eliminated the inductance of the starter from the arc circuit.

7. References

1.1 "Welding Processes and Workshop Automation, Public Session," Annual Meeting of the I.I.W., Bratislava, Czechoslovakia, 1979.

1.2 Vroman, A.R. and Brandt, H., "Feedback Control of GTA Welding Using Puddle Width Measurement," Welding Journal, Sept. 1976, pp. 742.

1.3 Nomura, et al., "Arc Light Intensity Controls Current in SA Welding System," Journal of Welding and Metal Fabrication, Sept. 1980, pp. 457-463.

3.1 Maecher, H., Z. Physik, Vol. 141, 1955, p. 198.

3.2 Szekely, J., Chang, C.W., "Electromagnetically Driven Flows in Metal Processing," Journal of Metals, Sept. 1976, pp. 6-11.

3.3 Emmons, H.W., "Arc Measurement of High-Temperature Gas Properties," The Physics of Fluids, Vol. 10, No. 6, Jan. 67, p. 1125-36.

3.4 Glickstein, S.S., "Arc Modeling for Welding Analysis," Preprints of the International Conference on "Arc Physics and Weld Pool Behavior," London, The Welding Institute.

3.5 Witze, P.O., "The Impulsively Started Incompressible Turbulent Jet," Sandia Laboratories, SAND 80-8617.

3.6 Abramovich, S., Solan, A., "The Initial Development of a Submerged Laminar, Round Jet," Journal of Fluid Mechanics, Vol. 59, Part 4, 1973, pp. 791-801.

3.7 Milne-Thompson, L.M., Theoretical Hydrodynamics, MacMillan, 1968.

3.8 Schlichting, H., Boundary Layer Theory, McGraw Hill, 1968.

3.9 Galler, D., Kusko, A., Converti, J., "A Fast Response Transistor Current Regulator for Welding Research," IEEE-IAS, 1981 Annual Meeting, Philadelphia, PA.

3.10 Landes, K., et al., "Evaluation of the Mass Flow Field and the Electric Current Density Field in a Free Burning TIG Similar Arc," Schweissen und Schneiden 0/81.

4.1 Katz, J., "Ultrasonic Measurement and Control of Weld Penetration," S.M. Thesis, Department of Mechanical Engineering, M.I.T., May, 1982.

4.2 Vroman, A.R. and Brandt, H., "Feedback Control of GTA Welding Using Puddle Width Measurement," Welding Journal, 55, Sept. 1976, pp.742-49.

4.3 Richardson, R.W., Gutow, D.A. and Rao, S.H., "A Vision Based System for Arc Weld Pool Size Control," Measurement and Control for Batch Manufacturing, ASME Special Publication, Nov. 1982.

4.4 Nomura et al. "Arc Light Intensity Controls Current in in SA Welding System," Welding and Metal Fabrication, Sept. 1980, pp. 457-463.

4.5 Garlow, D., "Closed-Loop Control of Full Penetration Welds using Optical Sensing of Backbead Width," S.M. Thesis, Department of Mechanical Engineering, M.I.T., June 1982.

4.6 Zacksenhouse, M. and Hardt, D.E., "Weld Pool Impedance Identification for Size Measurement and Control," to be published, Trans ASME, Journal of Dynamic Systems, Measurement and Control, 1983.

4.7 Zacksenhouse, M., "Control of Penetration in Gas Tungsten Arc Welding-A Puddle Impedance Approach," S.M. Thesis, Department of Mechanical Engineering, M.I.T., May 1982.

4.8 Weiner, J. B., "A Model Back Bead Width Dynamics for Full Penetration Weld Control," S.M. Thesis, Department of Mechanical Engineering, M.I.T., May 1983.

4.9 Reiff, J.D., "Closed-Loop Control of Backside Puddle Width in the Gas Tungsten Arc Weld Process," S.M. Thesis, Department of Mechanical Engineering, M.I.T., May 1983.

5.1 Dror, Y., "Calculations and Measurement at Weld Puddle Geometry in GTA Welding," S.M. Thesis, Department of Ocean Engineering, M.I.T., June 1981.

6.1 Galler, D., Kusko, A., Converti, J., "A Fast Response Transistor Current Regulator for Welding Research," IEEE-IAS, 1981 Annual Meeting, Philadelphia, PA.

8. Publications

8.1 Theses

1. Crothers, J.J., "Temperature Changes and Transients in a Sequential Welding Plate," S.B. Thesis, Department of Mechanical Engineering, M.I.T., June 1980.

2. Edelstein, P.G., "A Lumped-Element Model for the Automatic Arc-Welding Process," S.B. Thesis, Department of Mechanical Engineering, M.I.T., June 1980.

3. Dror, Y., "Calculations and Measurement at Weld Puddle Geometry in GTA Welding," S.M. Thesis, Department of Ocean Engineering, M.I.T., June 1981.

4. Converti, J., "Plasma Jets in Arc Welding,", Ph.D. Thesis, Department of Mechanical Engineering, M.I.T., August 1981.

5. Zacksenhouse, M., "Control of Penetration in GTA Welding - A Puddle Impedance Approach," S.M. Thesis, Department of Mechanical Engineering, M.I.T., June 1982.

6.* Katz, J., "Ultrasonic Measurement and Control of GTA Weld Penetration," S.M. Thesis, Department of Mechanical Engineering, M.I.T., June 1982.

7.* Garlow, D., "Closed Loop Control of Full Penetration Welds Using Optical Sensing of Back Bead Width," S.M. Thesis, Department of Mechanical Engineering, M.I.T., June 1982.

*The last two theses were not supported by funds related to the current research project.

8.2 Papers and Presentations

1. Converti, J. and Unkel, W., "Plasma Jet Momentum," 33rd Gaseous Electronics Conference, Norman, OK, October 1980.

2. Converti, J. and Unkel, W., "Hydrodynamic Transient in a Tip-Plane Arc Configuration," 34th Gaseous Electronics Conference, Boston, MA, October 1981.

3. Masubuchi, K., Hardt, D., Paynter, H.M. and Unkel, W., "Improvement of Reliability of Welding by In-Process Sensing and Control," ASM Conference on Trends in Welding Research in the United States, New Orleans, LA, November 1981.

4. Galler, D., Kusko, A., Converti, J., "A Fast Response Transistor Current Regulator for Welding Research," IEEE-IAS, 1981 Annual Meeting, Philadelphia, PA.

5. Masubuchi, K., Hardt, D., Paynter, H.M., Unkel, W., Converti, J. and Zacksenhouse, M., "Improvement of Fusion Welding through Modeling, Measurement and Real-Time Control," International Conference on Welding Technology for Energy Applications, Gatlinburg, TN, May 1982.

6. Hardt, D. and Zacksenhouse, M., "Full Penetration Weld Pool Impedance Identification for Size Measurement and Control," ASME 103rd Winter Annual Meeting, Phoenix, AZ, November 1982.

Appendix A

Welding Fabrication as a Control System

In this research program, efforts were made to develop techniques for closed-loop control of arc welding. Although control of the welding operation is the most important aspect of the automatic control of welding, it is perhaps worth considering the entire welding fabrication as a control system. Fig. A1 schematically shows welding fabrication as a control system. The welding fabrication as commercially exercised today can be regarded as a pre-programmed open-loop control system, since no explicit in-process control is performed during the welding operation, as explained below:

(1) In manual arc welding, the operator performs a certain degree of in-process control by watching the weld pool and manipulating the welding torch or the electrode. However, there is no way to verify that the operator has performed proper manipulations.

(2) In automatic arc welding, machines currently on the market have no adaptive control capabilities. Optimum welding conditions thus preselected are used in actual construction. Once welding has commenced, welding conditions (welding current, arc voltage, travel speed) are normally kept unchanged even though there are some variations in the joint geometry such as the root gap.

In order to obtain reliable welds under these conditions, many efforts are currently made in pre-qualification. They include qualifications of joint design, welding procedure tests, qualification of welders, etc. The basic philosophy behind these pre qualifications is to make certain that designs, materials, processes, and operators are well qualified for the job. Of course these pre-qualifications are performed in many activities. In aviation, for example, aircraft is certified, airport facilities are certified, and pilots are certified. What is unique in welding fabrication, however, is that no systematic control is exercised during the actual welding operation, which is the most critical part of welding fabrication.

After welding is completed, sometimes even several days later, welds are inspected. The inspections include visual inspection as well as more sophisticated non-destructive techniques including radiography, ultrasonic tests, magnetic particle tests, etc. The problem here is that even these inspections are judged subjectively by inspectors. For example, there is no exact, uniform manner of interpreting X-ray films of welds. If no irregularities are found during the non-destructive inspections, the weld is assumed to be satisfactory. On the other hand, if irregularities are found, the weld is sent back for repair. After the repair is done, the weld is normally inspected again. Since the structure is inspected after welding and repairs are made if necessary, a certain degree of closed-loop control is currently exercised during the welding fabrication.

In the days of welding fabrication, until around the 1950's, many welded structures were sent for service without sufficient inspections. During the

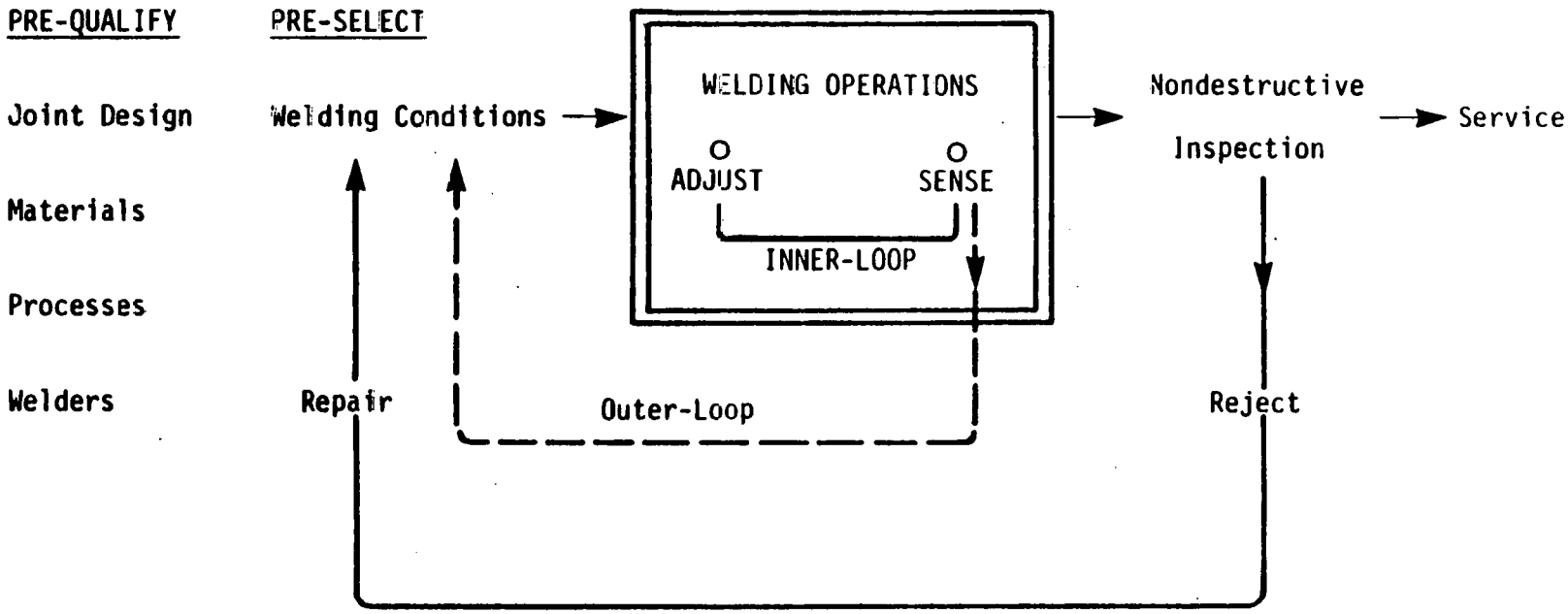

Figure A1 Welding Fabrication as A Control System

last 30 years, various new NDI techniques have been developed, and welds have been subjected to increasing numbers of inspections. At the same time, the demand for the reliability of welded structures has become increasingly stringent. Thus, the following have resulted over the years:

(1) In order to improve the reliability of welded structures without exercising in-process control, the requirements for pre-qualification have become increasingly exacting and complex.

(2) The percentage of repair work has increased resulting in a large increase in fabrication cost.

This explains why the M.I.T. research on the fundamentals of in-process control of welding is so important.

The primary objective of the in-process control of the welding operation is to produce weld metals free from defects. This is the most critical part of welding fabrication. However, in the construction of actual structures such as ships, pressure vessels, etc., engineers must control these other properties as well:

(1) Metallurgical properties of the weld metal and the heat-affected zone must be controlled so that the welded structure performs satisfactorily in services, and

(2) Residual stresses and distortion must be controlled so that excessive amounts of residual stresses and distortion are avoided.

The control of these properties may be called the "outer-loop" control, while the control of the weld metal productions may be called the "inner-loop" control. Although the major emphasis of the current M.I.T. research has been placed on the "inner-loop" control, which is the most critical part of welding automation, we believe that it is important to expand the scope of future research to cover some subjects related to the "outer-loop" control. As an example of what can be done on the "outer-loop" control, a brief description about the control of hydrogen-induced cracking is given below.

Control of Hydrogen-Induced Cracking of High-Strength Steel Weldments

The prevention of hydrogen-induced cracking is an important technical problem in welding high-strength steels. It has been proven that hydrogen-induced cracking occurs when the following conditions are met:

(1) The material used is insensitive to hydrogen-induced cracking.

(2) A sufficient amount of atomic or diffusable hydrogen exists in the weldment.

(3) A sufficient amount of tensile stress exists.

It is also well established that the cracking is a delayed phenomenon. In other words, a certain amount of time, as long as a week under certain conditions, is required before cracking occurs. Consequently, the following procedures are commonly used today for preventing hydrogen-induced cracking:

(a) Use base and weld metal with materials not sensitive to hydrogen-induced cracking. Several investigators have proposed formulas for estimating the sensitivity of a material to hydrogen-induced cracking [1,2]. For example, the carbon equivalent (CE) is commonly used to estimate the sensitivity of steel for hydrogen-induced cracking. A common formula:

$$CE = \%C + \frac{\%Mn}{4} + \frac{\%Ni}{20} + \frac{\%Cr}{10} + \frac{\%C}{40} - \frac{\%Mo}{50} - \frac{\%V}{10}$$

When CE by the above formula exceeds 0.40, underbead cracking can occur. Other investigators have also proposed various formulas for estimating hydrogen-induced cracking sensitivity of different steels [2].

(b) Use welding processes which produce only a low amount of hydrogen. For example, use gas metal arc welding process using argon shielding gas, or use low-hydrogen type electrodes.

The basic philosophy used today is to prevent cracking by selecting proper combination of parameters before welding. No attempt is made to prevent the cracking by controlling what happens during welding. Since hydrogen-induced cracking is a delayed phenomenon, we simply wait long enough before inspecting the weld. A common practice employed by various agencies including the U.S. Navy, is to wait one week. This procedure certainly slows down the welding fabrication. When defects are found after this one week delay, the structure is completely cold and all welding equipment has been moved to another location. Therefore, the entire process of preheating, welding and so on must be reactivated for welding repair.

M.I.T. researchers believe that more efficient control techniques can be developed by studying what goes on during and after welding. Through years of research on the mechanisms of hydrogen-induced cracking, we know that the major factors that cause hydrogen-induced cracking are: (1) the stress level, (2) hydrogen level, (3) temperature, and (4) time. The first factors have complex distributions in a weldment and they change with time. Moreover, hydrogen cracking occurs only under certain combinations of the above parameters.

As an example, Fig. A2 shows experimental results on HT80 steel using the rigid restraint cracking (RRC) test. HT80 steel is a Japanese high-strength steel with a minimum ultimate tensile strength of 80 Kg/mm^2 (113,800 psi). Further details of the RRC test may be found in Chapter 14 of a book by Masubuchi entitled Analysis of Welded Structures [1]. The degree of restraint of a joint is expressed in the terms of the restraint length. A butt joint with a shorter restraint length is more highly restrained.

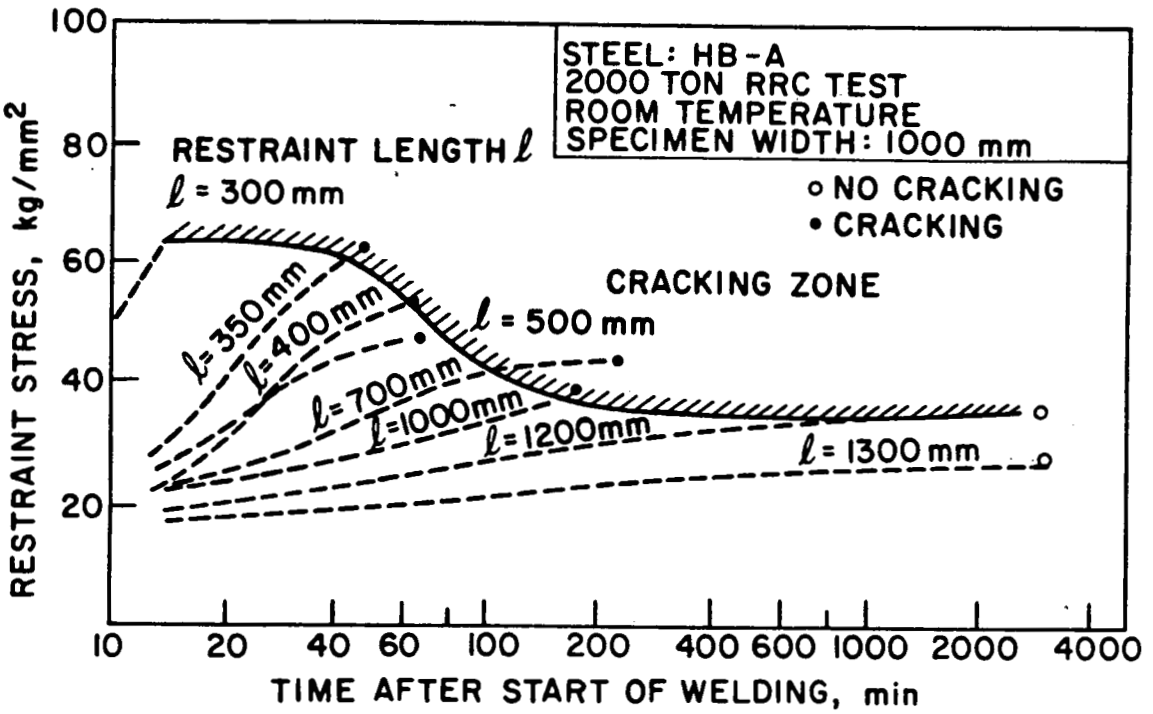

Figure A2 Development of Restraint Stress During Cooling and Cracking in the RRC Test.

When a joint is more highly restrained, higher stresses are produced in a shorter time causing hydrogen-induced cracking. It is interesting to note that it takes a considerably long time, around 20 to 200 minutes depending upon the degree of restraint, after welding is completed before reaction stresses are fully deveoped. When the reaction stresses are below a certain level, cracking does not occur even after a long period. This is why a weld is inspected even one week after welding is completed. Although the border line between cracking and non-cracking is shown by one curve in Fig. 2, it varies depending upon the level of hydrogen and material properties.

The results shown in Fig. 2 strongly suggest that it is possible to develop a technique for preventing hydrogen delayed cracking by controlling what happens during welding. For example, when a weldment is heated properly to diffuse hydrogen away, the critical stress for cracking can be raised so that the time-reaction stress relationship is maintained below the critical level. In other words, hydrogen-delayed cracking can be avoided by guiding the time-stress-hydrogen relationship of a weld through a "safe corridor" during and after welding.

Efforts are currently being made in another research program at M.I.T. to further verify this idea of controlling and preventing hydrogen-induced cracking in high-strength steel weldments. We believe that various systems can be developed to perform the "outer-loop" control of subjects involved in welding including the metallurgical properties of the heat-affected zone, residual stresses and distortion, etc.

References

[A1] Masubuchi, K., Analysis of Welded Structures, Pergamon Press, 1980.

[A2] Welding Handbook, Volume 1 Fundamentals of Welding, Seventh Edition, American Welding Society.